5-2013

Predicting the Onset of Cavitation in Nonsymetric Bifurcations

Steven E. Daniels

PREDICTING THE ONSET OF CAVITATION IN NONSYMMETRIC BIFURCATIONS

by

Steven E. Daniels

A thesis submitted in partial fulfillment
of the requirements for the degree

of

MASTER OF SCIENCE

in

Mechanical Engineering

Approved:

Dr. Robert E. Spall Major Professor	Dr. Michael C. Johnson Committee Member
Dr. Aaron Katz Committee Member	Dr. Mark R. McLellan Vice President for Research and Dean of the School of Graduate Studies

UTAH STATE UNIVERSITY
Logan, Utah

2013

Abstract

Predicting the Onset of Cavitation in Nonsymmetric Bifurcations

by

Steven E. Daniels, Master of Science

Utah State University, 2013

Major Professor: Dr. Robert E. Spall
Department: Mechanical and Aerospace Engineering

Many existing dams in the United States were built without hydroelectric generating accessories and are now being considered for hydroelectric installations. A bifurcation is regularly used as the method for diverting the water to the new generators. With a bifurcation installed as part of the new piping system, cavitation could become a problem. Although widely used, there are no published data on cavitation characteristics or head loss coefficients for these bifurcations. Dimensional analysis has not been adequate for experimentally quantifying the cavitation potential and full scale testing is prohibitive for many large geometries. Therefore this study utilized Computational Fluid Dynamics (CFD) in conjunction with a physical model to predict conditions that would cause the onset of cavitation. Head loss coefficients were also calculated from the CFD simulations and physical model. Based on these results, the authors have produced recommended operating conditions that will allow bifurcations to operate within safe limits of cavitation. This study was not exhaustive but presents data that has previously been unavailable and will assist designers and operators to better understand the performance of such bifurcations.

(91 pages)

Public Abstract

Predicting the Onset of Cavitation in Nonsymmetric Bifurcations

by

Steven E. Daniels

Many existing dams in the United States were built without hydroelectric generating accessories and are now being considered for hydroelectric installations. A bifurcation is regularly used as the method for diverting the water to the new generators. With a bifurcation installed as part of the new piping system, cavitation could become a problem. Cavitation can cause vibrations, damage, loss of efficiency, and excessive noise. Although widely used, there are no published data on cavitation characteristics or head loss coefficients for these bifurcations. Dimensional analysis has not been adequate for experimentally quantifying the cavitation potential and full scale testing is prohibitive for many large geometries. Therefore this study utilized Computational Fluid Dynamics (CFD) in conjunction with a physical model to predict conditions that would cause the onset of cavitation. Head loss coefficients were also calculated from the CFD simulations and physical model. Based on these results, the authors have produced recommended operating conditions that will allow bifurcations to operate within safe limits of cavitation. This study was not exhaustive but presents data that has previously been unavailable and will assist designers and operators to better understand the performance of such bifurcations.

Acknowledgments

I would like to thank all those who helped this work come to fruition. It has been a lot of work, some of which did not go as planned. My wife, especially, has given me much support and had to deal with many late nights and frustration. I would like to thank the Utah Water Research Laboratory for their resources and funding. Dr. Michael Johnson has been a great help in guiding me in my research and has kept me motivated through this project. Dr. Robert Spall has been a great help with CFD and the analysis of the results. Without these and others this project would not be what it is, thank you.

Steven E. Daniels

Contents

List of Tables

List of Figures

Notation

cfs	cubic feet per second
E	total energy
ft	feet
ft/s	feet per second
g	accelerator due to gravity
H_L	head Loss
in	inch
kg	kilogram
K	head loss coefficient
K_{branch}	head loss coefficient through the branch
K_{run}	head loss coefficient through the run
m	meter
p	pressure
p_{inlet}	average inlet pressure
p_{low}	lowest pressure in the domain
p_{ref}	reference pressure
$p_{shifted}$	pressure shift that makes $p_{low} = p_v$
p_v	vapor pressure
psi	pounds per square inch
$psig$	pounds per square inch, absolute
$psig$	pounds per square inch, gage
s	second
V	average velocity
V_{outlet}	average outlet velocity
y^+	wall y plus

z	elevation
α	kinetic energy correction factor
γ	specific weight
ρ	fluid density
σ	cavitation number
σ_o	onset of cavitation number

Grid Refinement Index Notation

e	error
GCI_{fine}	fine-grid convergence index/uncertainty
h	representative cell size
N	number of cells
p	apparent order
r	grid refinement factor/ratio
ϕ	relevant parameter

Chapter 1

Introduction

1.1 Motivation

There are many existing dams in the United States that were built without hydroelectric generating facilities. Many of these dams are now being considered for hydroelectric power generation because hydroelectric power represents a clean and renewable resource. Owners and operators are financially driven to pursue opportunities for energy production where feasible.

One way to divert water to new hydroelectric installations is to connect the new penstock to the existing outlet works piping. This is done so that the flow can be diverted to the generators without having to do major retrofits to the existing dam structure. This setup creates a nonsymmetric bifurcation, illustrated in Figure 1.1. Flow can be diverted through either penstock or the outlet works pipe in varying amounts depending on required release conditions and desired flow.

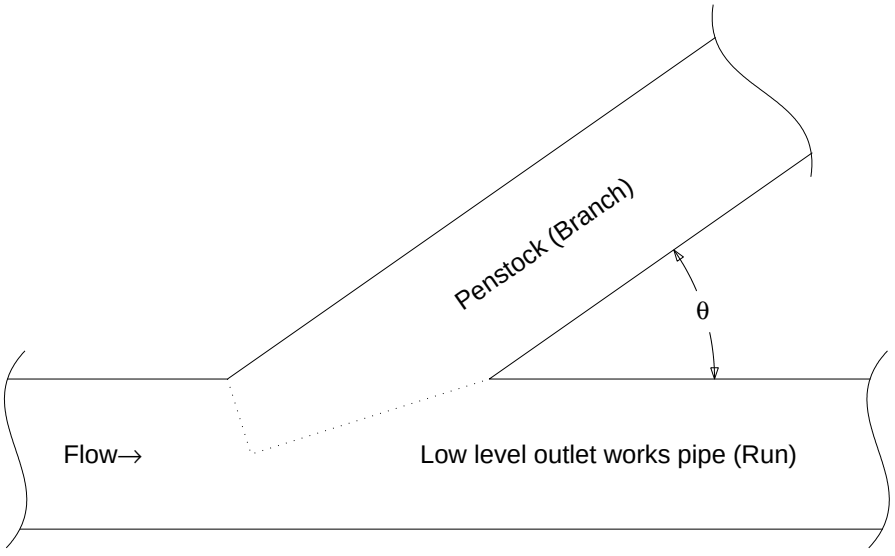

Fig. 1.1: Illustration of a nonsymmetric bifurcation

With a bifurcation installed as part of the new piping system, cavitation could become a problem at the connection to the existing pipe. Cavitation is the rapid vaporization of water and subsequent collapse of vapor bubbles upon exposure to higher pressures. Cavitation can cause vibrations, damage, loss of efficiency, and excessive noise. Because a bifurcation causes a rapid change in the flow direction which is accompanied by localized acceleration and corresponding low pressure, cavitation could develop under certain conditions. Owners and operators of installations where bifurcations are proposed need to understand the limitations of the bifurcation and where and under what conditions cavitation may occur. An important secondary motivation for this study is understanding the energy losses that occur due to nonsymmetric bifurcation as there are no published data on the energy loss for the bifurcations of this type.

The increased interest in hydroelectric installations on existing dams has lead to the present study which was commissioned to identify what hydraulic conditions for nonsymmetric bifurcations will be present at the onset of cavitation and also to quantify bifurcation head loss characteristics for the losses occurring through the run and through the branch.

1.2 Cavitation

Hydrodynamic cavitation is the formation of vapor bubbles in low pressure areas and subsequent bubble collapse when it travels to a higher pressure region. Small air or gas bubbles or debris in the liquid or on the boundary surface provide a source of nuclei for cavitation bubbles. To initiate cavitation a critical tension in the liquid is required. Pressures below the vapor pressure will cause tension on the fluid [1]. Knowing exactly what pressure will cause the critical tension is dependent on the liquid and amount of nuclei in the fluid. The more nuclei in a fluid the less tension can be sustained. In the case of water, and especially reservoir water, the quantity of nuclei present is substantial which results in the water being unable to sustain tension below that associated with its vapor pressure. Therefore cavitation will occur approximately when the pressure goes below the vapor pressure [2]. Although pressure does not fully capture the state of stress in a fluid [3], experimental results have shown that in industrial type flows cavitation will occur close to the vapor pressure [2].

1.2.1 Cavitation Number

The cavitation number (σ), as defined in Eq. (1.1), is commonly used to assess cavitation potential and severity [1, 2]

$$\sigma = \frac{p_{ref} - p_v}{\frac{1}{2}\rho V^2} \tag{1.1}$$

where p_{ref} is the reference pressure from a location up stream, p_v is the vapor pressure, V is the average velocity in the pipe and ρ is the density of the water. The reference pressure, p_{ref} for this study was located two diameter upstream from the hip. The variables, p_{ref} and p_v can be measured in gage or absolute pressure as long as they are consistent. σ has limitations but overall has been found to be a good parameter to use when reporting cavitation data [2, 4].

1.2.2 Onset of Cavitation

For this study we have defined the onset of cavitation (σ_o) when the cavitation is between the inception and constant cavitation. Constant cavitation, as defined for valves, has been determined to be a safe operational level [2, 4].

The cavitation number is an important parameter that enables designers to be able to predict when or if cavitation will occur during operation. If a calculated σ is greater than σ_o, then the bifurcation will operate without a harmful amount of cavitation. If the calculated σ is lower than σ_o, then the cavitation could start to cause damage to the bifurcation or the connecting penstock. For various states of cavitation, the Reynolds number can have differing effects on σ. When calculating the onset of cavitation at high Reynolds number, σ_o is virtually Reynolds number independent. This is because at high Reynolds numbers the flow is fully rough turbulent flow and inertial forces overwhelm the viscous forces. With inertial forces dominating the flow, the pressure difference will scale predominantly with the velocity squared [2].

1.3 Head Loss Coefficient

An important secondary motivation for this study is understanding the energy losses that occur due to a nonsymmetric bifurcation. The energy state of flow throughout a piping network is important in the design and operation of piping networks. The total head (E) at a location in a pipe can be

determined with

$$E = \frac{p}{\gamma} + z + \alpha \frac{V^2}{2g} \tag{1.2}$$

where p is the pressure, γ is the specific weight, z is the elevation above a selected datum, α is the kinetic-energy correction factor, V is the average pipe velocity, and g is the acceleration due to gravity. Since flow in this study was turbulent, α was assumed to be one in all calculations [5]. By taking the difference between the energy state upstream and the energy state downstream of a pipe fitting or geometry the total head loss from that fitting or geometry can be calculated. The nondimensional loss coefficient (K) can then be calculated with:

$$H_L = K \frac{V_{ref}^2}{2g} \tag{1.3}$$

In the present study the V_{ref} in Eq. (1.3) was defined as the velocity upstream of the bifurcation. The head loss coefficient can then be used to find H_L for other flow conditions with only the upstream velocity needed. For this study the head loss from the bifurcation was measured from two diameters upstream of the hip to six diameters downstream of the crotch.

1.4 Research Overview

It is not feasible to do full scale testing on bifurcations of the size that are used in outlet works piping for cavitation and head loss data. Therefore being able test a model and extrapolating the test data to full scale would be ideal. Dimensional analysis has allowed such testing to be done for many flow parameters on many geometries, including head loss. However, cavitation is an area of study that dimensional analysis has not been shown to accurately predict how σ_o scales with size. This is because there are more parameters relating to cavitation then can be accounted for. Consequently, geometric scaling effects for σ are unpredictable for geometries that have not previously been studied [1].

For this reason a combination of Computation Fluid Dynamics (CFD) in conjunction with a physical model was used in this study. A physical test and CFD simulation of the nonsymmetric bifurcation model was done to see how well the CFD would predict what would actually happen.

Then partial and full scale CFD simulations were done and the results from these simulations were extrapolated based on the results of the model test.

1.5 Research Objectives

The objectives of this study were be to determine σ_o and K for bifurcations that have 35, 45, and 60 degree bifurcation angles. The following are the tasks that were done to meet the objectives.

1. Conduct literature search
2. Test a physical model with a $4in$ diameter and 45 degree bifurcation angle for σ_o and K from 0 to 100 percent flow splits in 10 percent increments
3. Run simulations on the same geometry that was used for the physical test at flow splits from 0 to 100 percent
4. Run simulations on $8ft$ diameter pipe with a 35, 45 and 60 degree bifurcation angle, an average velocity of $15ft/s$, $30ft/s$ and $60ft/s$ will be used at flow splits from 0 to 100 percent.
5. Run additional simulations on $2ft$ diameter pipe with a 45 degree bifurcation angle
6. Use the Grid Convergence Index (GCI) to obtain numerical accuracy of the simulations
7. Create plots showing σ_o verses flow split
8. Create plots showing head loss coefficients out each outlet verses flow split

Chapter 2

Literature Review

Numerous studies have been done on cavitation for external and internal flows. Internal flow cavitation studies have mostly centered on cavitation caused by valves. After an extensive literature search, very little has been found that is applicable to the study at hand. What follows are sections of pertinent subjects related to this study with what literature could be found.

2.1 Onset of Cavitation

Knapp [1] determined that there are three factors that affect the inception of cavitation: (1) the characteristic of the impurities in the liquid which give rise to the nuclei; (2) The physical and thermodynamic properties of the liquid; (3) The hydrodynamic characteristics of the flow, that is, the pressure and velocity of the liquid and the physical size of the guiding surface.

Tullis [6] determined for orifices and valves that the onset of cavitation scale effects are independent of Reynolds number. Variations in pressure and or geometric size are the parameters that effects how the onset of cavitation will scale. logarithmic scaling equations were developed that allowed these scale effects to be accounted for. Tullis [2] also found that these logarithmic scaling effects have an upper limit at about $3ft$ in diameter, for valves larger than this size the scaling equation are not valid.

The American Water Works Association Manual (AWWA M49) [4] reported that constant cavitation is a safe level of cavitation. M49 also points out that because of the distinct noise associated with the constant level of cavitation, it can be discerned audibly with good accuracy.

2.2 Cavitation Studies Utilizing CFD

In recent years there has been an influx of CFD usage to help predict cavitation. Most of the CFD models that are in use or development try to capture all aspects of the cavitation using

methods such as the volume of fluid (VOF) method, and they usually are time dependent models. These studies, while useful, are not relevant to the current study at hand because the point of the current study is to use the pressure calculations from steady state simulations to predict the onset of cavitation based on Eq. (1.1). Therefore the myriad of studies that have used these types of CFD solvers has not been included here.

Glenn and Decker [7] used Star-CCM+ with the $k-\varepsilon$ turbulence model to predict the onset of cavitation for various valves. The onset of cavitation was predicted to occur when the lowest pressure in the domain dropped below the vapor pressure. They found that when compared to physical data, in most cases the CFD did a good job of predicting the onset of cavitation. The exception to this was when the cavitation was caused by high shear forces in the boundary layer. When this occurred the CFD result predicted the onset of cavitation to happen sooner then experimental results. This study is the only one of its kind that has used CFD in this manner to predict the onset of cavitation.

Feng [8] used a general purpose CFD code with a $k-\varepsilon$ turbulence model to study the cavitation number and flow characteristics of a double eccentric butterfly valve. The cavitation number from the CFD was in good agreement with the test data, though the flow was not driven to cavitation.

2.3 Head Loss in Nonsymmetric Bifurcations

The American Water Works Association Manuel (AWWA M49) [4] reported that for 100 percent of the flow through the branch of a 45 degree angle bifurcation the loss coefficient should be about 1.25.

Sadrnezhad [9] studied nonsymmetric bifurcations for the Karun I second power station project. The nonsymmetric bifurcation studied had a smooth conically shaped outlet branch to minimize eddies with a bifurcation angle of 48.46 degrees. The legs of the bifurcation had smaller diameters then the upstream diameter.

The American Iron and Steel Institute [10] reported head loss coefficients for 60 degree angle nonsymmetric bifurcations with the branch having a smaller diameter than the run.

There is no published data that could be directly compared with the results of the current study,

with the exception of the coefficient given by AWWA which is only for a 100 percent of the flow going through the branch for a single bifurcation angle.

2.4 Head Loss Studies Utilizing CFD

CFD has been used extensively to study fluid mechanics for many geometries. Below are a few examples where CFD was used to analyzed performance factors for internal flow situations.

Hollingshead [11] used CFD to predict discharge coefficients for venturi, standard concentric orifice plate, v-cone, and wedge flow meters at small Reynolds numbers. He also performed high Reynold number simulations for comparison with published data and found good agreement.

Del Toro [12] studied a $48in$ diameter butter fly valve at various valve openings and flow conditions and found very good agreement when comparing the head loss coefficients with the physical test.

Sibilla [13] studied a nozzle check valve using CFD and gives a good summary of references to other studies using CFD to predict flow characteristics and performance factors for several geometries. He found that the computational model must rely on a properly designed mesh with adequate grid nodes in the regions of high-pressure gradients and of high velocity gradients. Insufficient meshing can lead to overestimation of the valve flow coefficient.

Chapter 3

Experimental Setup and Result

All physical data for this study was collected at the Utah Water Research Laboratory (UWRL). The objectives of the experiment were to determine values of σ_o, K_{run} and K_{branch} at 10 percent increments of flow rate split.

3.1 Physical Model

The physical model was fabricated using acrylic so that cavitation could be visually verified. The model had a $4in$ in diameter and had a 45 degree angle bifurcation. Figure 3.1 shows the computer model that was used fabricate the model. The inlet to the model was one diameter upstream of the hip and the legs extended two diameters down from the crotch. At the crotch and hip a radius of 1/96 the pipe diameter was used to smooth the transition from the main pipe to the branch. This corresponds to what would be seen on a full scale bifurcation. A technical drawing is included in Appendix B, Figure B.1.

3.2 Test Setup and Procedure

The acrylic model was bolted to pipes at the inlet connecting face and the outlet connecting faces to complete a simple pipe network for testing purposes as shown in Figure 3.2. Pressure taps were located two diameters upstream from the hip and six diameters downstream of the crotch in each leg. These locations were based on guidelines given by the Instrument Society of America [14]. Valves were located in the run and branch more than 20 diameters downstream of the crotch for flow regulation. A pump supplied water through the bifurcation at velocities ranging from $36 ft/s$ to $50 ft/s$ resulting in a Reynolds number range of 0.7 to 1 million. The valves were adjusted so that the desired flow split and σ_o were occurring simultaneously. The cavitation was also audibly discerned. This was done because of the distinct noise associated with the incipient and constant

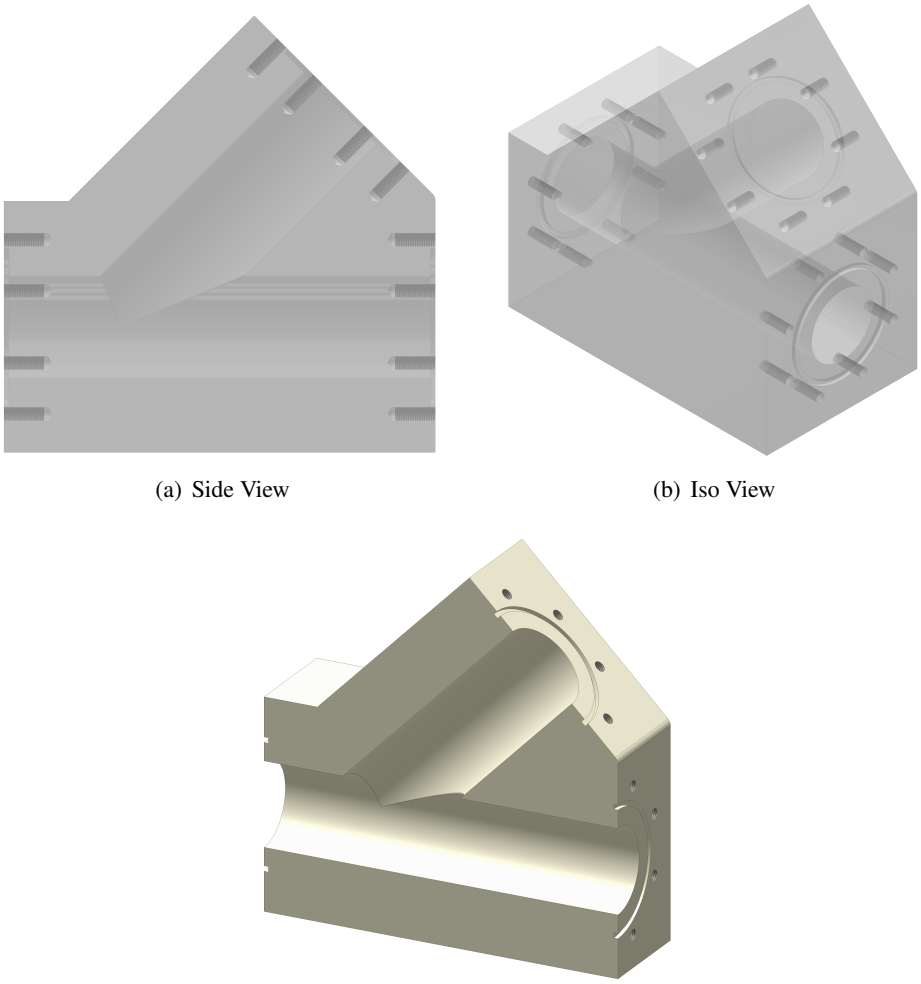

(a) Side View

(b) Iso View

(c) Section View

Fig. 3.1: CAD illustration of the bifurcation test model.

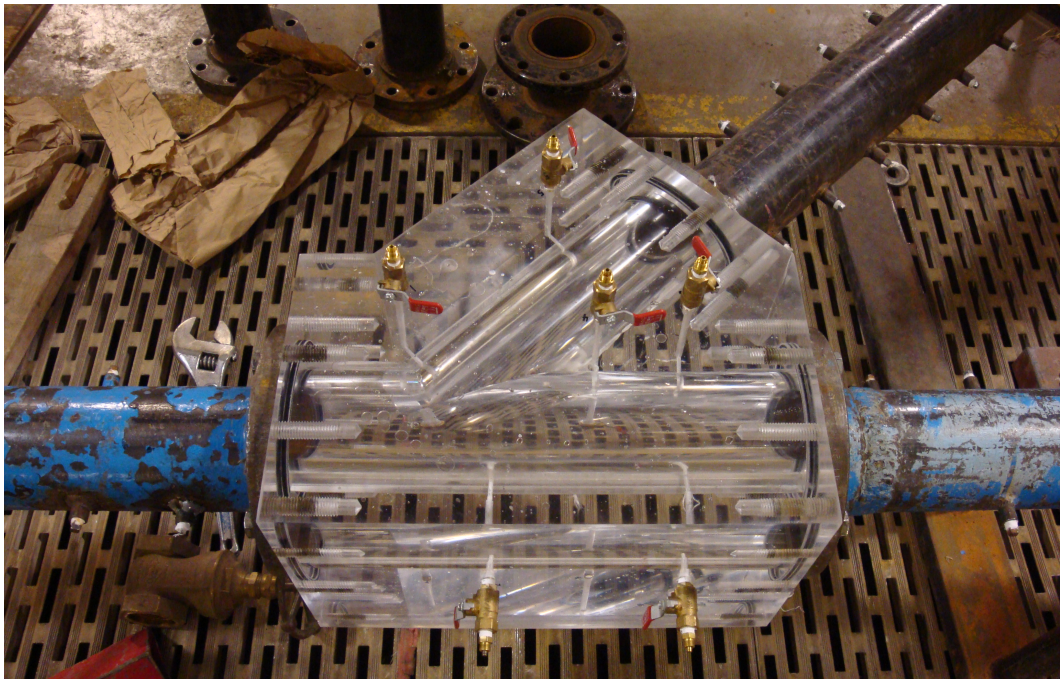

Fig. 3.2: Physical bifurcation model in testing pipe network.

levels of cavitation [4]. Pressures and flow rate were measured for each condition investigated. Calibrated flow meters were located upstream of the bifurcation and in the run. The flow in the branch was calculated using conservation of mass. The gage pressure was measured from each pressure tap and the barometric pressure was added to the upstream pressure for calculating σ_o in terms of absolute pressures.

3.3 Experimental Uncertainty

The uncertainty analysis of the physical data followed ASME PTC 19.1-2005 [15]. The flow meters measured flow rate in gpm and the uncertainty was 0.25 percent. Pressure reading were in $psig$ and had an uncertainty of 0.1 percent. These uncertainties were propagated to the uncertainty of K through the equation for K along with the uncertainty of the pipe area and specific weight of the water. Detailed calculations are shown in Appendix D. During the testing the water temperature was 39.9 degrees Fahrenheit, and the barometric pressure was $12.61 psia$.

The uncertainty of σ_o cannot be specifically quantified, but based on the experience of Dr. Johnson, the uncertainty of σ_o from the audible observation was estimated to be within 5 percent.

3.4 Results

Table 3.1 shows the pressure readings that were taken at each flow split with the associated upstream velocity. Table 3.2 shows the calculated σ_o at each flow split. Tables 3.3 and 3.4 are the calculated K_{run} and K_{branch}, respectively. Included are the uncertainties in both percent and absolute. Plots of σ_o and K are in the CFD results chapter for comparison with the CFD results, see Figures 5.2 and 5.6.

To visually verify where the cavitation was occurring the cavitation was allowed to go well beyond σ_o at a few flow splits. The location of the cavitation was seen predominantly on the branch side of the crotch, with some occurring at the hip. All the cavitation occurred at the center line of the bifurcation. As an example a video recording was taken for a 30 percent flow split. Intermittent cavitation clouds could were observed. Figure 3.3 shows side by side pictures from the video, the left figure shows a cavitation cloud, and the right figure is just after the cloud disappeared.

Table 3.1: Pressure readings from physical model test.

Upstream Velocity (ft/s)	Flow Through Branch (%)	Upstream Pressure (psig)	Pressure in Run (psig)	Pressure in Branch (psig)
45.90	0.00	3.41	0.84	3.48
50.24	9.49	2.19	3.71	3.53
49.72	20.18	3.09	7.91	6.00
48.23	29.73	5.76	12.47	9.30
47.75	39.50	6.77	14.98	10.93
45.24	49.50	10.80	19.67	14.83
42.75	60.47	15.66	23.79	18.11
41.30	69.82	18.19	26.08	19.33
40.03	79.87	20.48	27.75	19.91
38.50	89.94	23.19	29.51	20.66
36.14	100.00	27.21	27.69	22.71

Table 3.2: Calculated σ_o from physical model test.

Upstream Velocity (ft/s)	Flow Through Branch (%)	σ_o
45.90	0.00	1.12
50.24	9.49	0.86
49.72	20.18	0.94
48.23	29.73	1.16
47.75	39.50	1.25
45.24	49.50	1.69
42.75	60.47	2.29
41.30	69.82	2.67
40.03	79.87	3.05
38.50	89.94	3.57
36.14	100.00	4.51

Table 3.3: Calculated K_{run} and uncertainty from physical model test.

Flow Through Branch (%)	K_{run}	Uncertainty of K_{run}	Uncertainty of K_{run} (%)
0.0	0.1812	0.00663	3.66
9.5	0.0914	0.00624	6.83
20.2	0.0702	0.00578	8.23
29.7	0.0772	0.00541	7.01
39.5	0.0985	0.00508	5.15
49.5	0.1006	0.00504	5.01
60.5	0.1816	0.00484	2.66
69.8	0.2208	0.00487	2.20
79.9	0.2845	0.00486	1.71
89.9	0.3559	0.00500	1.40
100.0	0.4190	0.00565	1.35
	Median:	0.00508	3.66
	Mean:	0.00540	4.11
	Standard Deviation:	0.00061	2.48
	Max:	0.00663	8.23
	Min:	0.00484	1.35

Table 3.4: Calculated K_{branch} and uncertainty from physical model test.

Flow Through Branch (%)	K_{branch}	Uncertainty of K_{branch}	Uncertainty of K_{branch} (%)
0.0	0.9949	0.00081	0.08
9.5	0.9126	0.00051	0.06
20.2	0.7852	0.00119	0.15
29.7	0.6851	0.00181	0.26
39.5	0.5725	0.00247	0.43
49.5	0.4621	0.00330	0.71
60.5	0.4345	0.00395	0.91
69.8	0.4127	0.00453	1.10
79.9	0.4143	0.00515	1.24
89.9	0.4451	0.00589	1.32
100.0	0.5123	0.00696	1.36
	Median:	0.00330	0.71
	Mean:	0.00332	0.69
	Standard Deviation:	0.00216	0.52
	Max:	0.00696	1.36
	Min:	0.00051	0.06

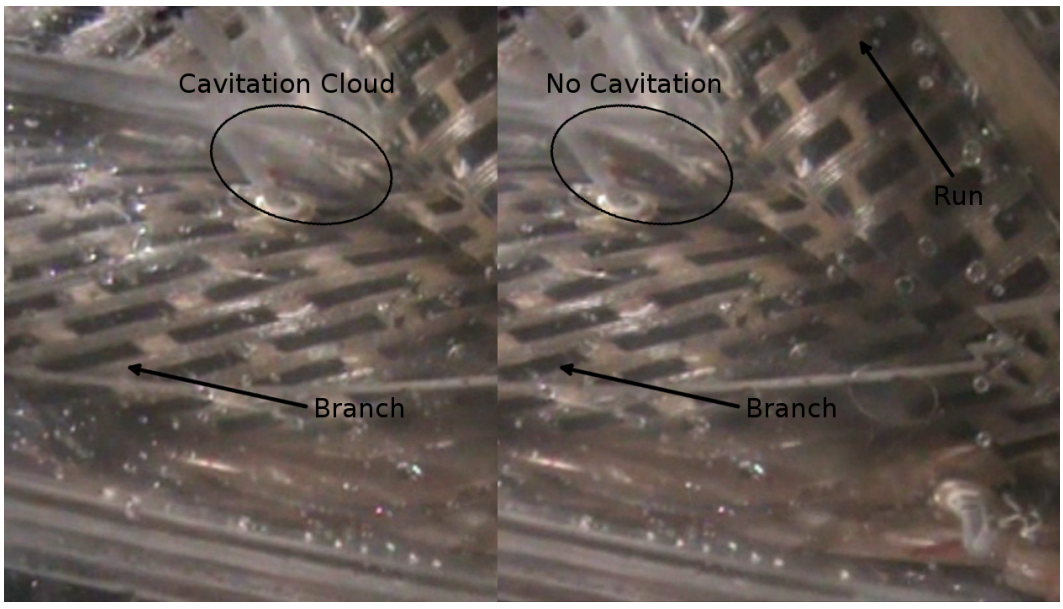

Fig. 3.3: Cavitation cloud near crotch with 30 percent flow through the branch.

Chapter 4

Computational Fluid Dynamics

STAR-CCM+ [16], a commercially available general purpose Computation Fluid Dynamics (CFD) package, was used for the CFD simulations in this study. This chapter outlines the specific CFD setup used for the present study, as well as CFD calculation considerations. It is assumed that the reader has at least a basic understanding of CFD. Detailed explanations of the concepts and workings of STAR-CCM+ can be found in the users manual [16].

4.1 Geometry and Boundary Conditions

The geometries for the simulations were modeled in Star-CCM+'s integrated 3D-CAD software. The following are the parameters that were used in defining the domain and boundary conditions for the CFD simulations. The inlet was located two diameters upstream from the hip with fully developed velocity and turbulence quantity profiles as inlet boundary conditions. The outlets were located six diameters downstream of the crotch with a split flow outlet condition; this allowed a percentage of the flow to be specified for each outlet. An illustration of the domain is shown in Figure 4.1. The bifurcations that were modeled were symmetric about the horizontal plane as shown in Figure 4.2. This was taken advantage of by splitting the domain in half with a symmetry plan, cutting the simulation time by 50 percent. Consistent with the physical model, at the hip and crotch a radius of 1/96 of the pipe diameter was used to smooth the transition of the split. This provided a 1 in radius for the 8 ft diameter pipe as would be done on a fabricated bifurcation to eliminate sharp corners. Three bifurcation angles were simulated for this study, 35, 45, and 60 degrees. Figure 4.3 shows the three angles side by side. Three diameter sizes were studied, $4in$, $2ft$, and $8ft$, with a 45 degree angle bifurcation.

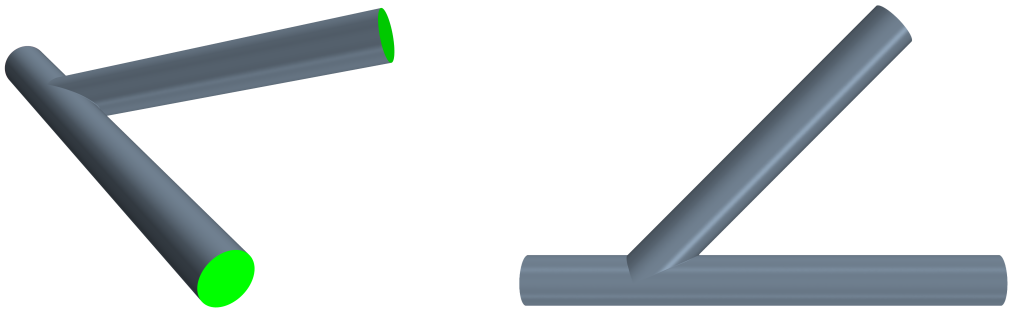

Fig. 4.1: CFD bifurcation model.

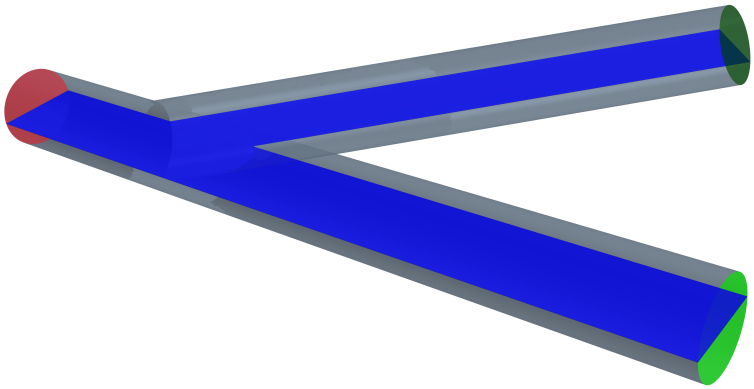

Fig. 4.2: Bifurcation symmetry, indicated by blue plane.

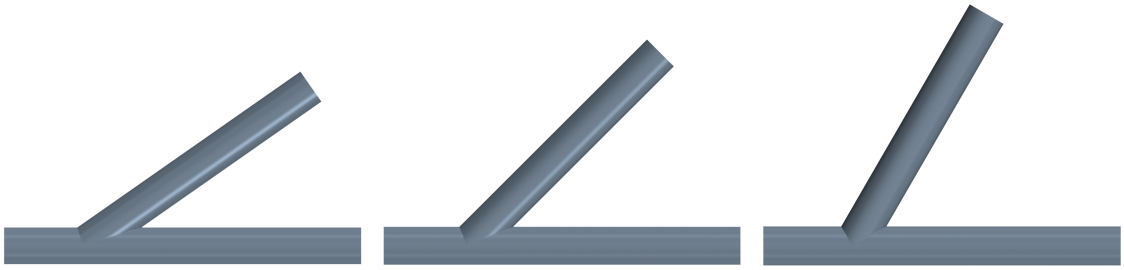

(a) 35 degree angle (b) 45 degree angle (c) 60 degree angle

Fig. 4.3: Bifurcation angles studied.

4.2 Meshing

Finite volume meshing was done in STAR-CCM+ using the Polyhedral, Prism layer and Extruder meshers. These were all controlled with reference values in the meshing options.

4.2.1 Polyhedral Mesh

Polyhedral meshes provide a balanced solution for complex mesh generation problems. They are relatively easy and efficient to build, requiring no more surface preparation than the equivalent tetrahedral mesh. The polyhedral cells created typically have an average of 14 cell faces.

4.2.2 Prism Layer Mesh

The prism layer mesher is used to generate orthogonal prismatic cells next to wall boundaries. Prism layers allow high-aspect-ratio cells to be used in the mesh, thus providing better cross-stream resolution without incurring an excessive stream-wise resolution. Prism layers are critical to properly resolving turbulent boundary layers. Figure 4.4 shows the prism layers on the inlet face along with the polyhedral core mesh.

The parameters that are used to define the prism layers are the thickness, number of cells, and stretch factor. The prism layers geometrically grow larger as they move away from the wall, this allows for a better transition to the core mesh.

The wall y^+ parameter is a nondimensional number that is dependent on the prism layers and fluid velocity, it is used to help determine how well the boundary layer is being resolved. For this study knowing the pressures near the wall was critical, to help accomplish this a low wall treatment was used. This means that wall y^+ values need to be on the order of unity. A finer prism layer will

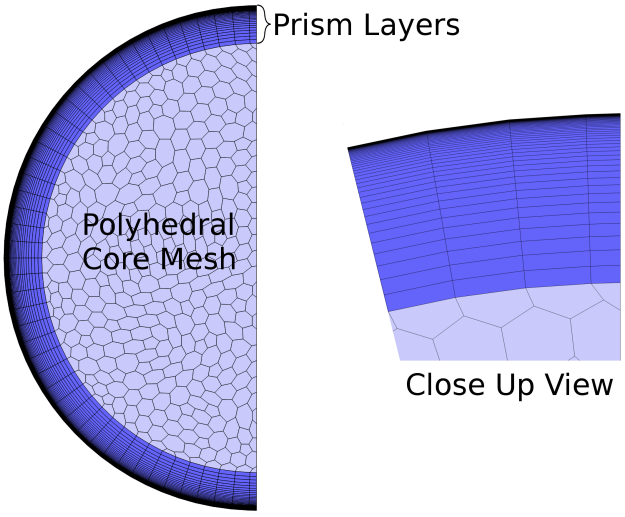

Fig. 4.4: Prism layers and polyhedral core mesh on inlet face.

result in a lower wall y^+. The wall y^+ cannot be determined before a simulations is completed. An initial exploratory simulation must be run and then the result iterated on until a desired wall y^+ is found.

For this study a prism layer calculator was created in SMath Studio to help find the proper number of cells and stretch factor in a systematic way, a print out of the file is shown in Appendix A. After an initial simulation run the y^+ values were analyzed to see if an adjustment was needed. If an adjustment was needed then the first cell thickness was adjusted and the prism layer calculator would output the needed stretch factor. This way there was no arbitrary guessing of the stretch factor for a given cell thickness.

The sharp transition from the run to branch creates a high velocity region, because of this, finer prism layers were needed to keep the y^+ low in this region. This fine grid region was defined by the fine volume grid refinement as shown in Figure 4.5.

For this study it was found that for the $2ft$ and $8ft$ diameter pipe with a velocity of $30ft/s$ the first prism layer should be $1.5 \times 10^{-5} ft$ thick for the main volume and $0.6 \times 10^{-5} ft$ thick for the fine grid region. For the $4in$ diameter pipe with a velocity of $45ft/s$ the first prism layer should be $1.0 \times 10^{-5} ft$ thick for the main volume and $0.4 \times 10^{-5} ft$ thick for the fine grid region.

4.2.3 Extruder Mesh

The extruder mesher allows a boundary located in a region continuum to be extended beyond its originally constructed bounds. This is particularly useful since the extended domain can be produced as orthogonal extruded cells which are ideal in steady internal flow in a pipe. The extruder mesher was used on the two outlets to extend the outlets $0.1ft$ for the $8ft$ diameter simulations and $0.05in$ for the $4in$ diameter simulations. This was done so that orthogonal cells would be at the boundary. This helped orient the velocity vectors normal to the boundary.

4.2.4 Volume Grid Refinement

Volume grid refinement was used to refine the mesh in the area around the connection of the pipes and especially the seam. This was done so that the cells would properly represent the geometry, and because this area was expected to have high pressure and velocity gradients. Figure 4.5

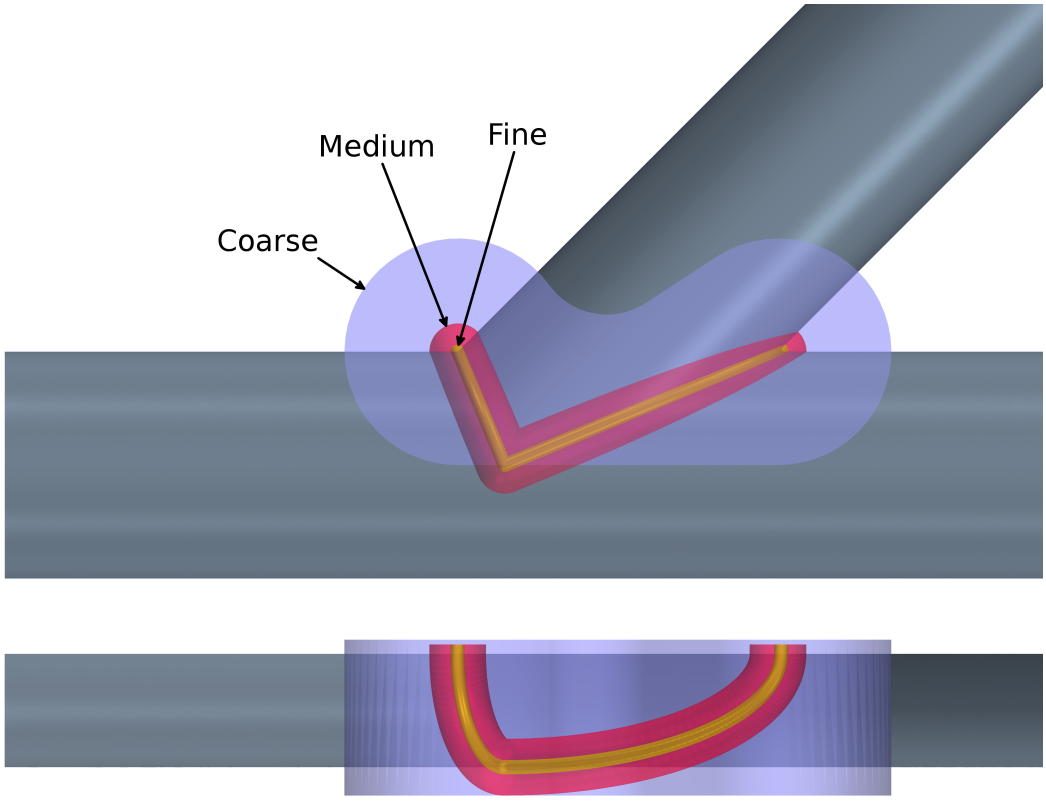

Fig. 4.5: Grid refinement volumes, top and side views.

shows the three refinement volumes that were used. The coarse, medium, and fine volumes had a 70, 40, and 8 percent reduction in cell size, respectively, compared to the base size.

4.2.5 Mesh Reference Values and Illustrations

Three mesh sizes were used for the grid refinement studies. Mesh 1 has the smallest cells, mesh 2 has medium cells and mesh 3 has the largest cells. Figure 4.6 shows representative cell sizes on the inlet face for each mesh used. Figure 4.7 shows representative cell sizes around the crotch, these cells are 8 percent of the base cell size in order to resolve the radius at the crotch. Figure 4.8 shows mesh 1 on the symmetry plane. Figure 4.8(b) is a close up so that the volume refinement can be seen more clearly.

Tables 4.1-4.3 show the reference values for each meshing option used for this study. Other option are available in STAR-CCM+ but these were left at their default values and do not significantly contribute to the meshes.

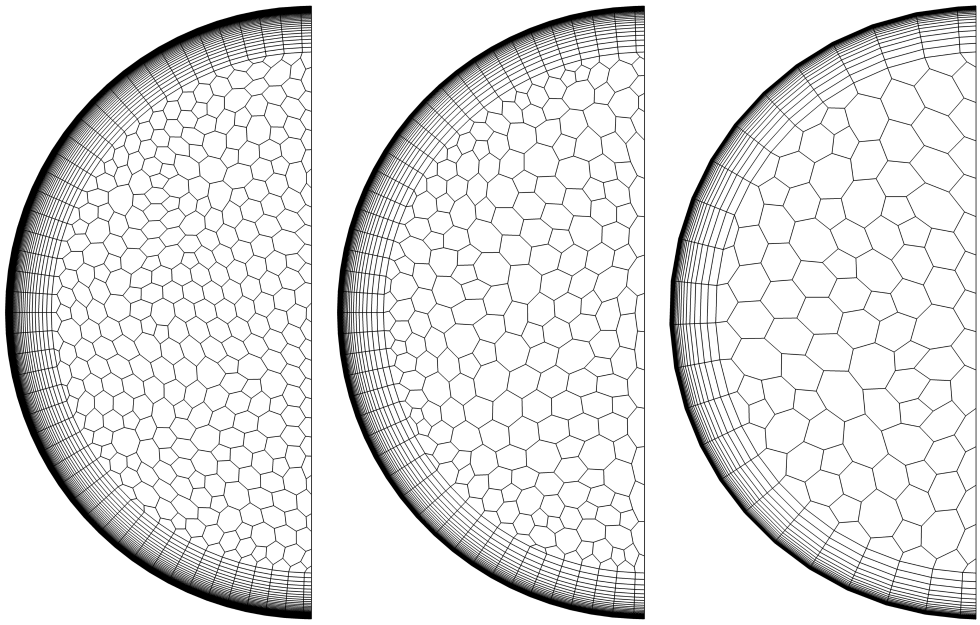

(a) Mesh 1 (Fine) (b) Mesh 2 (Medium) (c) Mesh 3 (Coarse)

Fig. 4.6: Mesh refinement illustration, inlet face.

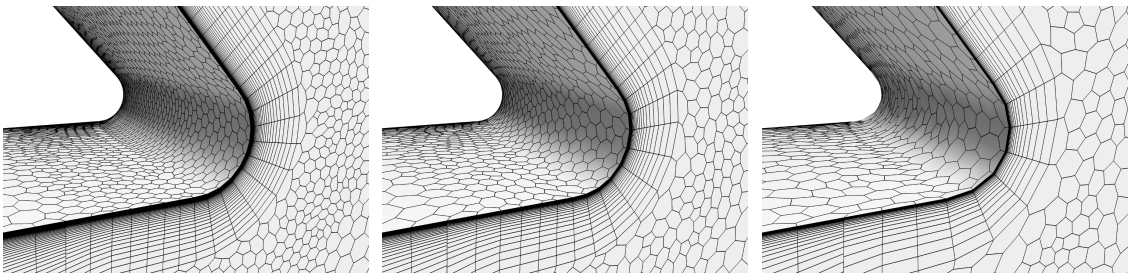

(a) Mesh 1 (Fine) (b) Mesh 2 (Medium) (c) Mesh 3 (Coarse)

Fig. 4.7: Mesh refinement at crotch.

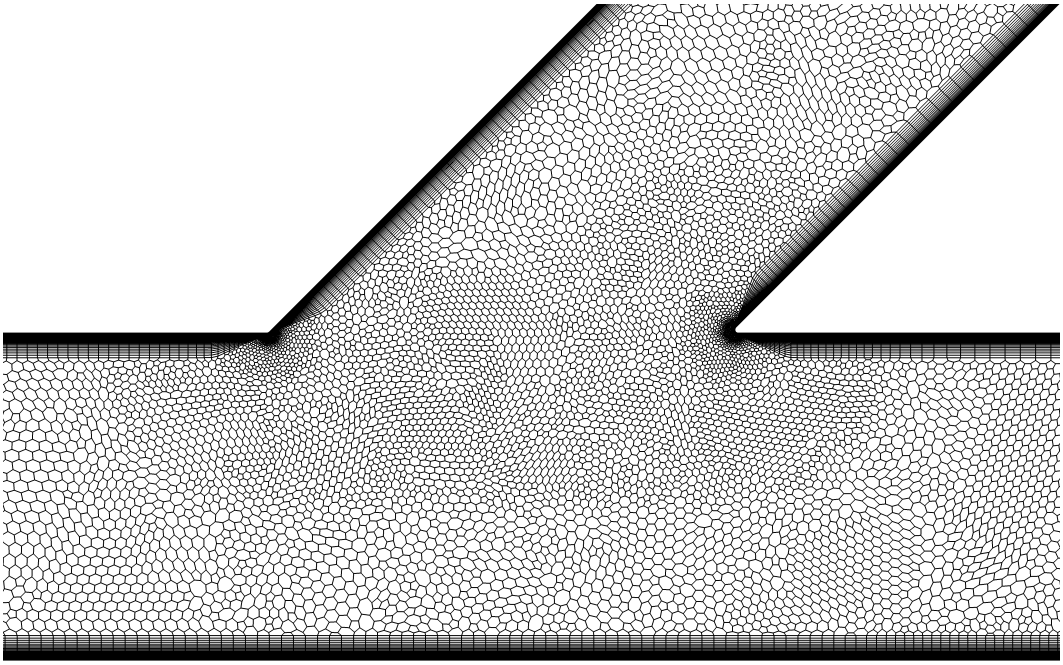

(a) Partially zoomed in

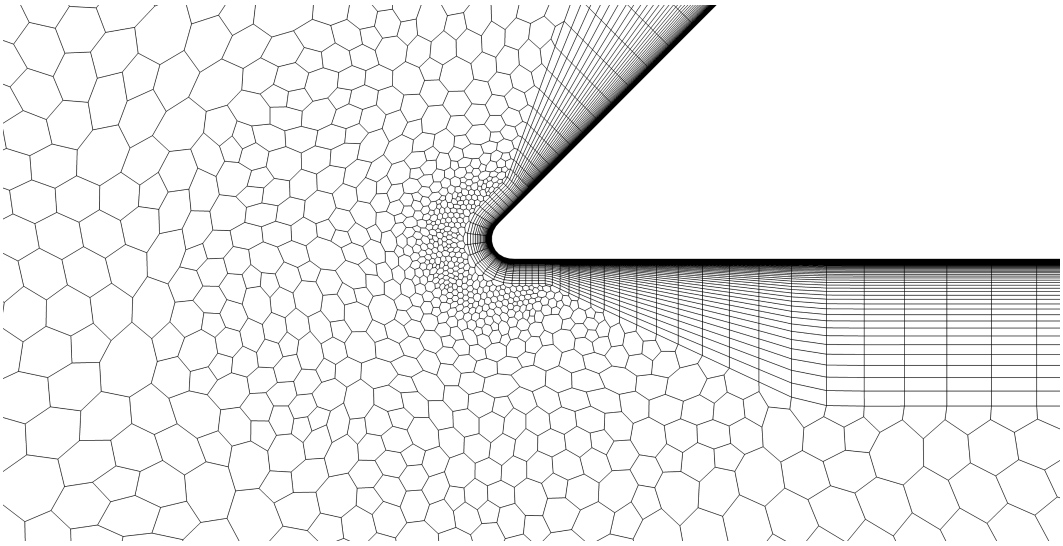

(b) Zoomed into medium refinement volume

Fig. 4.8: Mesh 1 on symmetry plane.

Table 4.1: $8ft$ diameter mesh reference values.

Option	Reference Value		
	Mesh 1	Mesh 2	Mesh 3
General Reference Values			
Base Size	0.28 ft	0.375 ft	0.50 ft
Number of Prism Layers	78	58	44
Prism Layer Stretching	1.114076	1.163563	1.230587
Prism Layer Thickness	0.6 ft	0.6 ft	0.6 ft
Coarse Volumetric Control			
Custom Size	70%	70%	70%
Medium Volumetric Control			
Custom Size	40%	40%	40%
Fine Volumetric Control			
Custom Size	8%	8%	8%
Number of Prism Layers	60	45	34
Prism Layer Stretching	1.137665	1.197156	1.282401
Prism Layer Thickness	0.1 ft	0.1 ft	0.1 ft

Table 4.2: $2ft$ diameter mesh reference values.

Option	Reference Value
General Reference Values	
Base Size	0.07 ft
Number of Prism Layers	64
Prism Layer Stretching	1.114075
Prism Layer Thickness	0.15 ft
Coarse Volumetric Control	
Custom Size	70%
Medium Volumetric Control	
Custom Size	40%
Fine Volumetric Control	
Custom Size	8%
Number of Prism Layers	49
Prism Layer Stretching	1.138607
Prism Layer Thickness	0.025 ft

Table 4.3: 4*in* diameter mesh reference values.

Option	Reference Value		
	Mesh 1	Mesh 2	Mesh 3
General Reference Values			
Base Size	0.141 in	0.189 in	0.252 in
Number of Prism Layers	54	40	30
Prism Layer Stretching	1.109620	1.162022	1.237267
Prism Layer Thickness	0.3 in	0.3 in	0.3 in
Coarse Volumetric Control			
Custom Size	70%	70%	70%
Medium Volumetric Control			
Custom Size	40%	40%	40%
Fine Volumetric Control			
Custom Size	8%	8%	8%
Number of Prism Layers	40	30	22
Prism Layer Stretching	1.130972	1.193717	1.298219
Prism Layer Thickness	0.05 in	0.05 in	0.05 in

4.3 Physics

The steady, incompressible, Reynolds-averaged Navier-Stokes equations were used in this study. Second-order upwinding was used for the convective terms for all transport equations. Pressure-velocity coupling was accomplished using the SIMPLE algorithm. The density was set to $1.9397 slugs/ft^3$ ($999.7 kg/m^3$) and the kinematic viscosity was set to $1.4073 \times 10^{-5} ft^2/s$ ($1.3074 \times 10^{-6} m^2/s$) these values correspond to water at 50 degrees Fahrenheit

4.4 Turbulence Models

Two turbulence models were used for this study, the $k-\varepsilon$ turbulence model and the $\overline{v^2}-f$ turbulence model.

4.4.1 $k-\varepsilon$ Turbulence Model

The $k-\varepsilon$ model is a two-equation model in which transport equations are solved for the turbulent kinetic energy and its dissipation rate. Various forms of the $k-\varepsilon$ model have been in use for several decades, and it has become the most widely used model for industrial applications. The Realizable $k-\varepsilon$ Two-Layer model was used in this study.

4.4.2 $\overline{v^2}-f$ Turbulence Model

The $\overline{v^2}-f$ is a four-equation model that is an extension of the $k-\varepsilon$ model. This model has been demonstrated to better predict separated flows, over the $k-\varepsilon$ model [17–19].

4.5 Fully Developed Simulations

The fully developed flow inlet conditions were obtained from separate two dimensional axisymmetric simulations that had a 10 diameter long straight pipe using a fully developed periodic interface between the inlet and the outlet. A mass flow was specified that would give the desired average velocity. Figure 4.9 shows an example plot from STAR-CCM+ of the velocity profile for an $8ft$ diameter pipe with an average velocity of $30ft/s$.

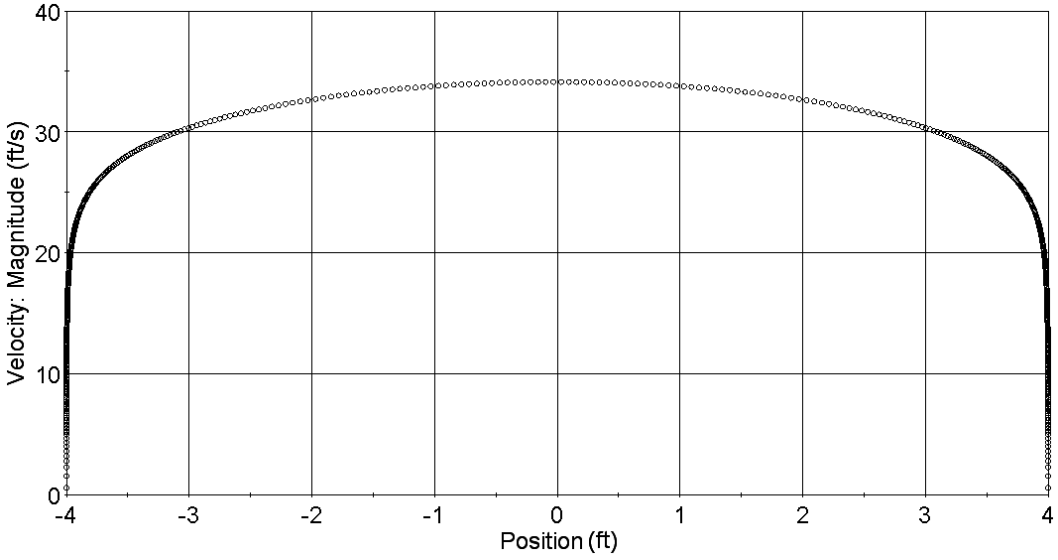

Fig. 4.9: Velocity profile from developed flow simulation $8ft$ diameter using $\overline{v^2}-f$ model.

4.6 CFD Calculations

4.6.1 Calculating σ_o

The lowest pressure that can be sustain by a fluid before cavitation is the vapor pressure, and only the pressure difference is important when the fluid is modeled as incompressible. Therefore

the pressure field was shifted so that the lowest pressure in the domain was equal to p_v. From the shifted pressures σ_o can be calculated using Eq. (1.1) with the following definitions:

$$\begin{aligned} p_v &= p_{low} + p_{shift} \\ p_{ref} &= p_{inlet} + p_{shift} \end{aligned} \tag{4.1}$$

where p_{low} is the lowest pressure in the domain, p_{inlet} is the inlet pressure, and p_{shift} is the needed pressure shift to make $p_{low} = p_v$. Subbing the above definitions into Eq. (1.1) gives:

$$\sigma_o = \frac{(p_{inlet} + p_{shift}) - (p_{low} + p_{shift})}{\frac{1}{2}\rho V^2} \tag{4.2}$$

This equation can be simplified so that p_{shift} disappears, giving:

$$\sigma_o = \frac{p_{inlet} - p_{low}}{\frac{1}{2}\rho V^2} \tag{4.3}$$

This equation was implemented in the CFD simulations to calculate σ_o

4.6.2 Calculating K

By using Eq. 1.2 and 1.3 the following was used to calculate K:

$$K = \frac{\frac{2g(p_{inlet} - p_{outlet})}{\gamma} + (V_{ref} - V_{outlet})}{V_{ref}^2} \tag{4.4}$$

The pressures, p_{inlet} and p_{outlet}, were calculated from the average pressure on the inlet and outlet faces. V_{ref} was specified for the simulation (either $30 ft/s$ or $45 ft/s$) and V_{outlet} was calculated based on the flow split.

4.6.3 Numerical Uncertainty

There are two parts that effect the numerical uncertainty of a simulation, iterative convergence and grid resolution.

Iterative Convergence

ASME [20] recommends that the normalized residuals decrease at least 4 orders of magnitude for iterative convergence. For the simulations using the $\overline{v^2}-f$ model the residuals decreased at least 6 orders of magnitude and most of them decreased 10 orders of magnitude. For the simulations using the $k-\varepsilon$ model the residuals decreased at least 4 orders of magnitude. An additional criteria for the convergence in this study was that all calculated values of σ_o and K remained constant in the 7th significant digit.

Grid Convergence Index

Numerical uncertainty was calculate on about half the simulations by doing a grid refinement study using the GCI approach set forth by ASME [20].

A summary of the recommended procedure are as follows:

1. Define a representative cell, mesh or grid size h

2. Select three significantly different sets of grids, and run simulations to determine the values of key variables important to the objective of the simulation study. It is desirable that the grid refinement factor, $r = h_{coarse}/h_{fine}$, be greater than 1.3. This value of 1.3 is based on experience, and not on formal derivation.

3. Let $h_1 < h_2 < h_3$ and $r_{21} = h_2/h_1$, $r_{32} = h_3/h_2$, and calculate the apparent order, p, of the method.

4. Calculate the extrapolated values

5. Calculate and report the error estimates.

For a detailed explanation of the above list see [20]. The calculations for this study are Appendix C. Tabulated values of the GCI results will be presented in the Results chapter.

Chapter 5

Results

The CFD results were obtained for flow splits ranging from 0 to 100 percent at 20 percent intervals with the $\overline{v^2}-f$ turbulence model simulations, 10 percent interval were used for the $k-\varepsilon$ turbulence model simulations. Five geometries were used in this study. The first three were $8ft$ in diameter with 35, 45 and 60 degree bifurcation angles. The remaining two each had a 45 degree bifurcation angle, one of $2ft$ diameter, and the other of $4in$ diameter. A velocity of $30ft/s$ was used in the $8ft$ and $2ft$ diameter bifurcations giving Reynolds numbers of 17 million and 4.3 million, respectively. A velocity of $45ft/s$ was used in the $4in$ diameter bifurcation giving a Reynolds number of 1 million. This velocity represents the average of the velocities from the physical test. Two additional simulations were done with $15ft/s$ and $60ft/s$ on the 8 ft diameter, 45 degree angle bifurcation with a 60 percent flow split. This was done to determine whether or not the σ_o would be independent of Reynolds number, and to determine the effect of Reynolds number on K.

5.1 $\overline{v^2}-f$ model verses $k-\varepsilon$ model

The research for this project started with setting up and running CFD simulations using the $k-\varepsilon$ turbulence model. The physical testing was conducted after many of the simulations had been completed. Results from the CFD were drastically different from the experimental result. For some reason the velocity around the crotch was accentuated when using the $k-\varepsilon$ model and this drove the local pressure down causing a much higher σ_o then was observed experimentally. This result led to an investigation of other turbulence models that could be used instead of the $k-\varepsilon$ model. The $\overline{v^2}-f$ model was chosen to replace the $k-\varepsilon$ model. This model is known to do better with predicting separation in flows [17–19]. Figure 5.1 shows the physical test data with the CFD results for the $4in$ diameter 45 degree angle bifurcation using both the $k-\varepsilon$ and the $\overline{v^2}-f$ models. The $\overline{v^2}-f$ model is not perfect but does a much better job of replicating the experimental data then the $k-\varepsilon$ model. All

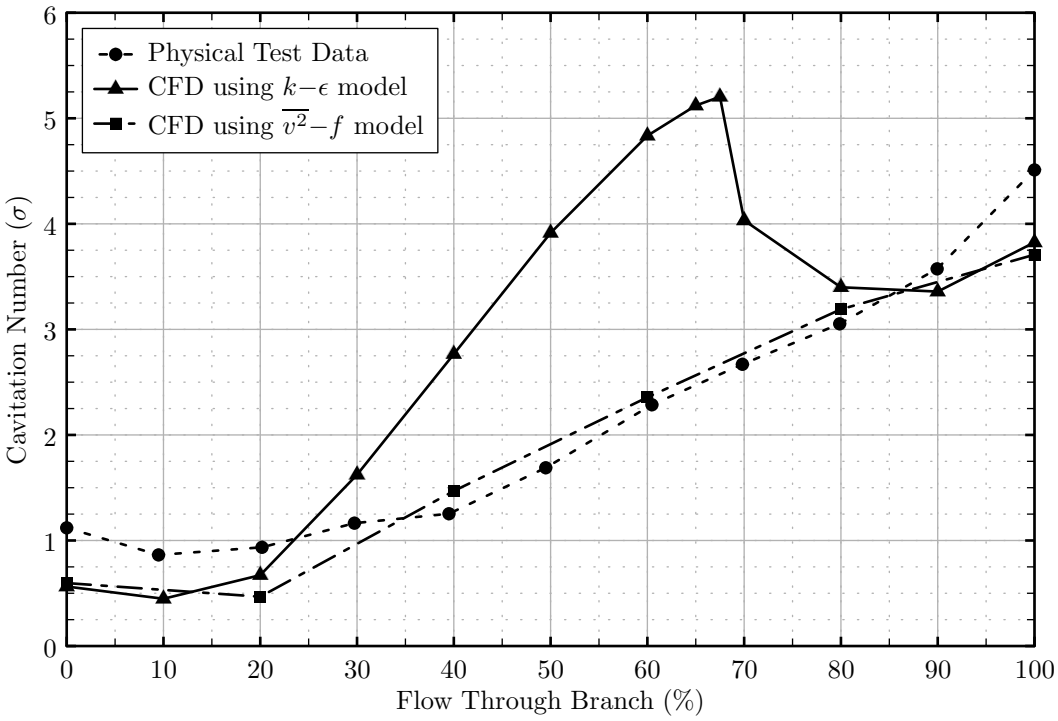

Fig. 5.1: $k-\varepsilon$ model verses $\overline{v^2}-f$ model verses physical test data of σ_o for 45 degree angle bifurcation.

CFD results presented from this point on will only be from simulation that used the $\overline{v^2}-f$ turbulence model.

5.2 The Onset of Cavitation

To best illustrate the cavitation results a plot of the experimental results along with the numerical results for the 45 degree angle bifurcations is shown in Figure 5.2. The onset of cavitation, σ_o, from the 4*in* CFD model matched the experimental results very well at 40, 60 and 80 percent flow splits. However, at the 0, 20 and 100 percent flow splits the CFD results are well below the experimental results. CFD simulations were also performed for a 2 ft diameter and 8 ft diameter bifurcation. These results show a slight scale effect of σ_o increasing as the diameter increased for the 20-80 percent flow splits. At 0 and 100 percent split σ_o was essentially unchanged for all three diameters. Figure 5.2 also include an Author's Recommendation line. This was added to rectify the differences in the CFD and physical data and also take in to account the scale effects seen in the CFD results.

The recommended line was obtained by adjusting the CFD results for the $8ft$ diameter simulation at each 20 percent increment and then a spline fit to adjust data point. If a shift in the $4in$ CFD data is done to match the physical test data then an equivalent shift in the $8ft$ CFD data should also be done. This is because the bifurcations are geometrically similar and the major factor effecting the onset of cavitation is the pressure field in the flow. If there is a difference between the CFD and the physical model at one size that same difference would be expected for other sizes. The following is the reasoning behind each data point adjustment for the author's recommended σ_o line.

- 0 Percent. To make the CFD results for the $4in$ simulation match the physical data a positive shift of about 0.5 was needed, because the $2ft$ and $8ft$ had no scale effect in the CFD result the recommended line for the $8ft$ diameter was shifted the same amount as the $4in$ diameter shift.

- 20 Percent. To make the CFD results for the $4in$ simulation match the physical data a positive shift of about 0.5 was needed, because the $2ft$ and $8ft$ had a scale effect in the CFD result the recommended line for the $8ft$ diameter was shifted up the by amount the $4in$ diameter shift was plus the scale effect.

- 40 and 60 Percent. Here the CFD result was slightly more conservative then the physical data, because of this there was no shift to the CFD data.

- 80 Percent. Here the CFD result was slightly more conservative then the physical data so no shift in the data point was needed, but a small positive shift was add to make the transition to 100 percent smoother.

- 100 Percent. Here the situation was same as the 0 Percent split except the shift is about 0.8.

The recommended line is conservative and can be used for other diameter bifurcations, but as the diameter decreases the recommended line becomes more conservative

Shown in Figure 5.3 are the CFD results for the $8ft$ diameter bifurcation with angles of 35, 45 and 60 degrees. The figure reveals a few notable trends. First, at 0 percent flow σ_o at each angle is within 9 percent of the mean. This indicates that even though this data is low compared with the

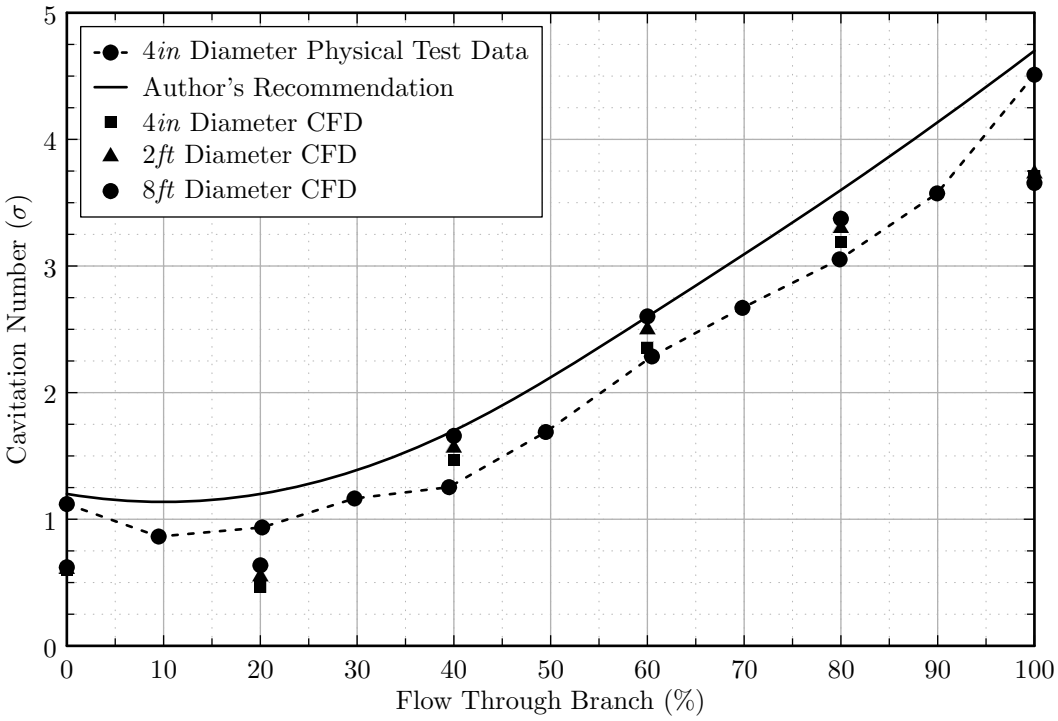

Fig. 5.2: Onset of cavitation for 45 degree angle bifurcations.

experimental results (for the 4 in diameter pipe), at each bifurcation angle σ_o will be approximately equal at 0 percent flow. The second trend is at 100 percent flow where, as the bifurcation angle increases, σ_o also increases. From 35 to 45 degrees the increase is 0.98 and from 45 to 60 degrees the increase is 0.85. This indicates that if the CFD results for the 45 degree angle bifurcation are shifted to match the physical data (as was done in Figure 5.2) then the CFD results for the 35 and 60 degree angle bifurcations should be shifted by the same amount.

Figure 5.4 shows the CFD and authors recommendation for the 35 degree angle $8ft$ diameter bifurcation. The exact same reasoning for the author's recommendation for the 45 degree angle bifurcation was used for the 35 degree angle bifurcation along with the considerations discussed for Figure 5.3. A notable difference between the trend of the 35 and 45 degree angle bifurcation is the hump that occurs around 50 percent flow split. In the CFD simulation it was noted that the velocity near the crotch was higher in the 35 degree angle simulation than the 45 degree angle simulation. This results in a lower pressure in the 35 degree angle simulation causing σ_o to be higher then the 45 degree angle simulation.

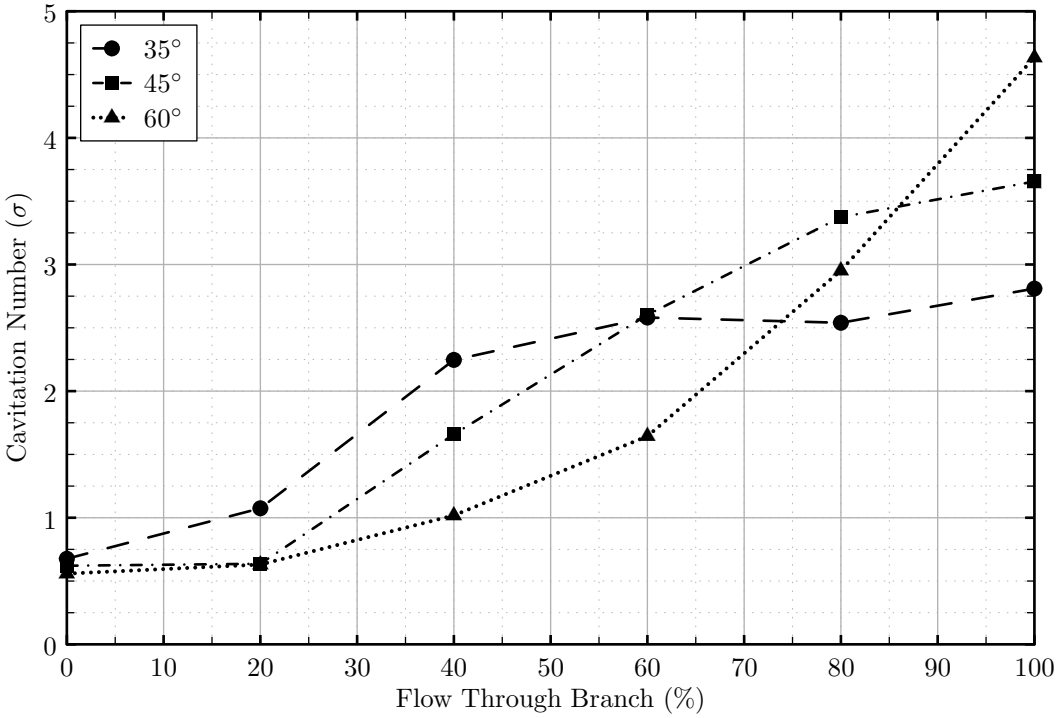

Fig. 5.3: Onset of Cavitation from $8ft$ diameter CFD simulation.

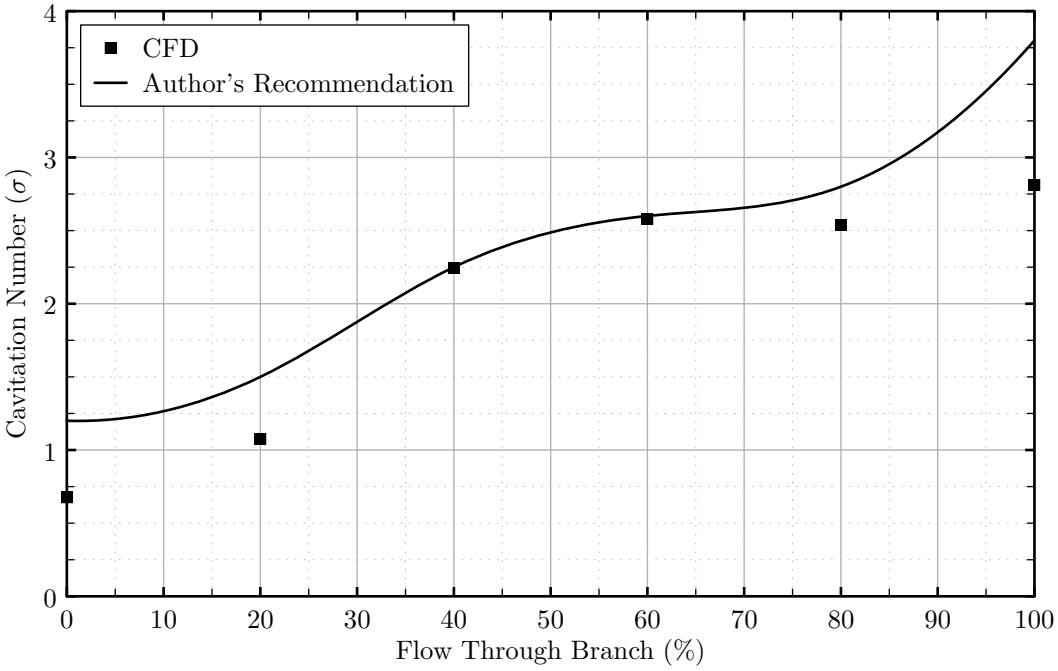

Fig. 5.4: Onset of Cavitation for $8ft$ diameter 35 degree angle bifurcation.

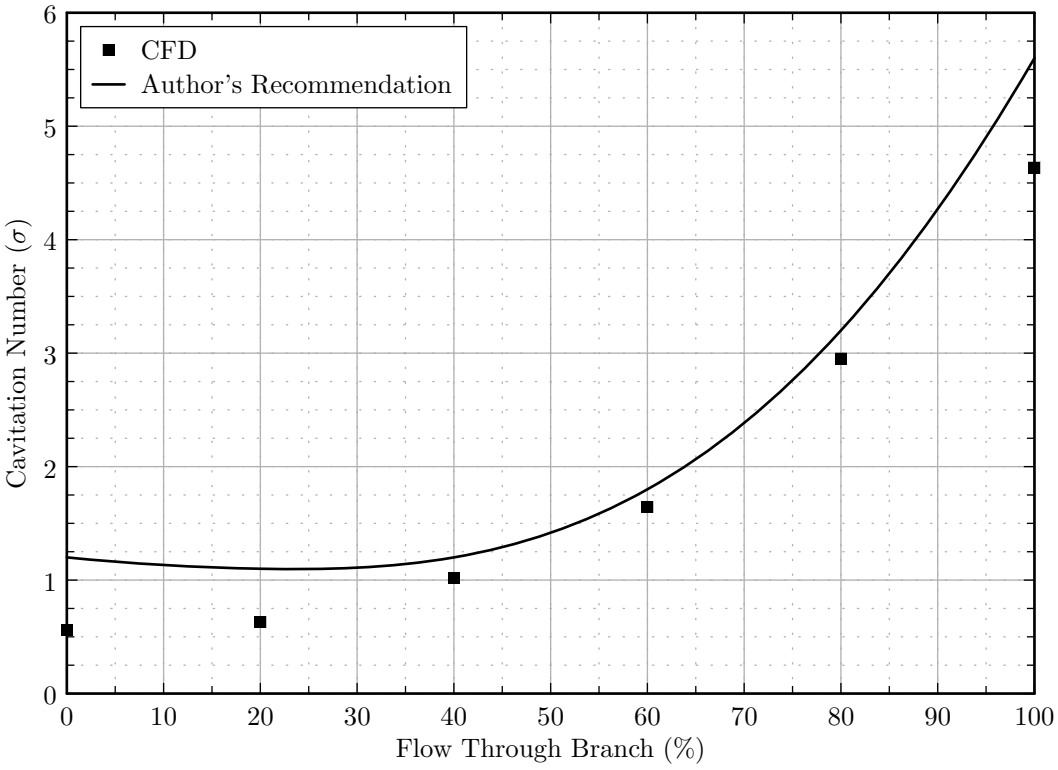

Fig. 5.5: Onset of Cavitation for $8ft$ diameter 60 degree angle bifurcation.

Figure 5.5 shows the CFD and author's recommendation for the 60 degree angle $8ft$ diameter bifurcation. The exact same reasoning for the author's recommendation for the 45 degree angle bifurcation was used for the 60 degree angle bifurcation along with the considerations discussed for Figure 5.3.

The additional simulations that were done with the 45 degree angel $8ft$ diameter bifurcation at $15ft/s$ and $60ft/s$ to check Reynolds number independence against the $30ft/s$ simulation varied by less than 2 percent, indicating Reynolds number independence. Generally, the numerical model showed that the cavitation occurred at the crotch of the bifurcation. This observation was substantiated with the physical model.

5.3 Head Loss Coefficient

Head loss coefficients are shown in Figure 5.6 for the 45 degree angle bifurcations. The CFD results indicate a distinct Reynolds number effect on K. That is, as the Reynolds number increases

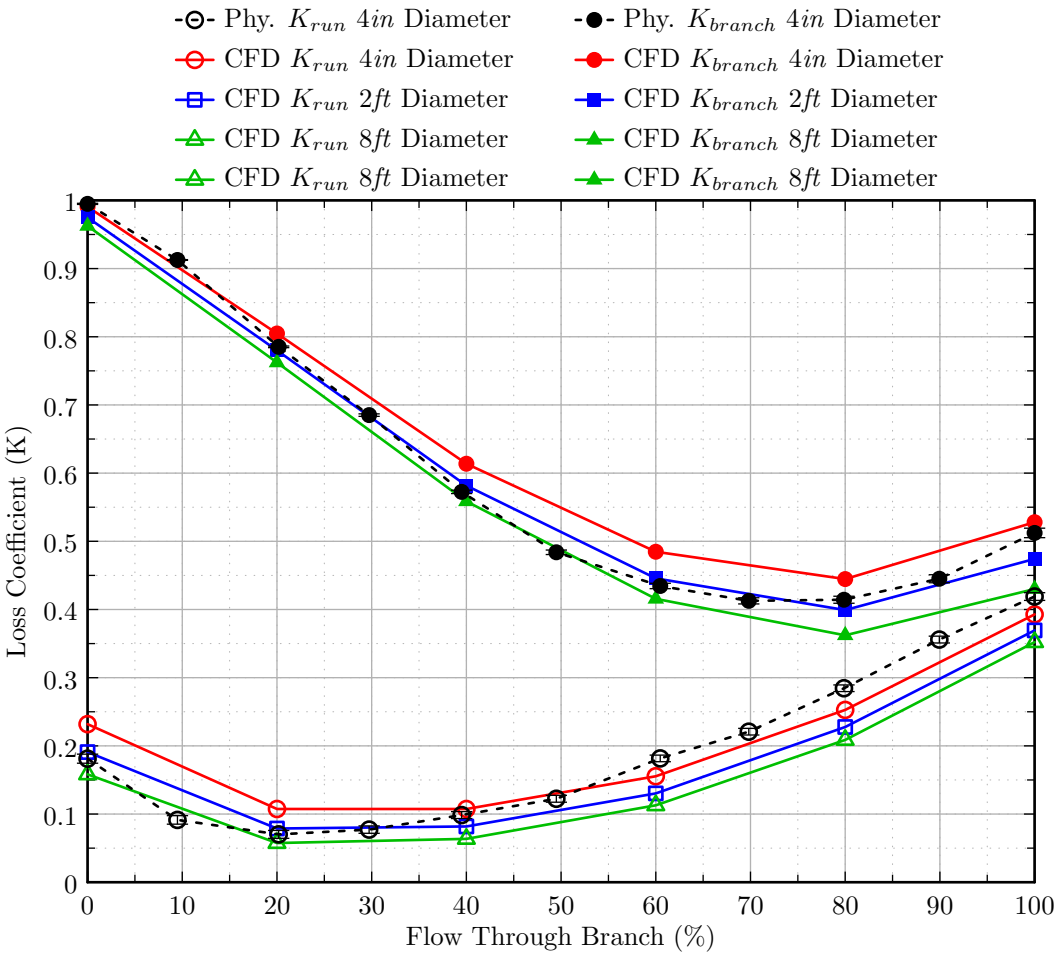

Fig. 5.6: Head loss coefficient for 45 degree angle bifurcation.

K decreases. This same trend was also observed for simulations that were done at $15ft/s$ and $60ft/s$ at 60 percent flow split. Figure 5.7 shows K for the $8ft$ diameter bifurcations with of 35, 45, and 60 degree angles. The head loss coefficients through the run, K_{run}, do not vary much with the bifurcation angle, while K_{branch} varies greatly with the bifurcation angle, increasing with the increase in angle. Losses through the run are a minimum when flow through the branch is roughly 20 percent. Conversely, losses through the branch are a minimum when flow through the branch is roughly 80 percent, independent of bifurcation angle.

For numerical values used in Figures 5.2-5.7 please refer to Table 5.1 where a summary of the CFD results for the onset of cavitation and head loss coefficients are given.

Table 5.1: Summary of CFD results for σ_o.

Flow Through Branch (%)	σ_o	K_{run}	K_{branch}
45° angle 4*in* diameter 45*ft/s* velocity			
0	0.597	0.232	0.991
20	0.467	0.107	0.805
40	1.469	0.107	0.614
60	2.356	0.155	0.485
80	3.191	0.253	0.445
100	3.708	0.393	0.528
45° angle 2*ft* diameter 30*ft/s* velocity			
0	0.605	0.191	0.975
20	0.547	0.079	0.780
40	1.563	0.082	0.582
60	2.499	0.130	0.446
80	3.298	0.228	0.399
100	3.729	0.369	0.474
45° angle 8*ft* diameter 30*ft/s* velocity			
0	0.621	0.158	0.963
20	0.636	0.057	0.762
40	1.659	0.064	0.559
60	2.602	0.113	0.416
80	3.374	0.209	0.362
100	3.656	0.352	0.430
35° angle 8*ft* diameter 30*ft/s* velocity			
0	0.676	0.179	0.933
20	1.075	0.061	0.718
40	2.246	0.067	0.495
60	2.581	0.113	0.344
80	2.540	0.201	0.299
100	2.810	0.337	0.399
60° angle 8*ft* diameter 30*ft/s* velocity			
0	0.559	0.145	0.978
20	0.630	0.054	0.815
40	1.018	0.059	0.657
60	1.644	0.111	0.551
80	2.952	0.215	0.518
100	4.635	0.362	0.567

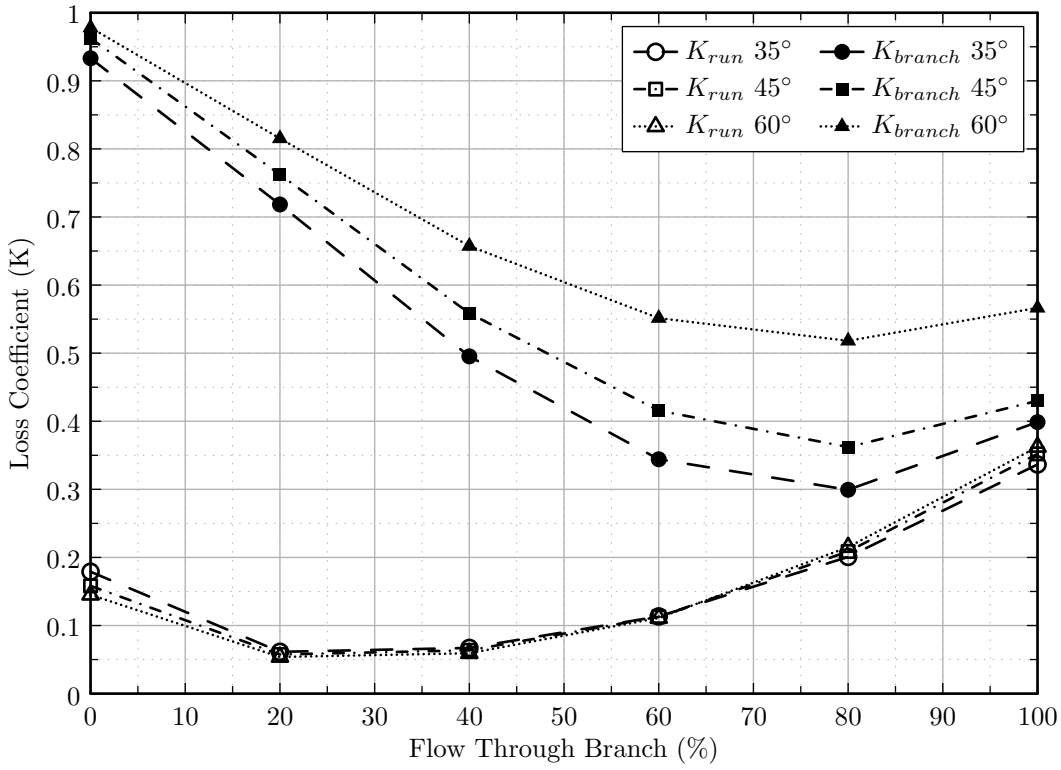

Fig. 5.7: Head loss coefficient for $8ft$ diameter bifurcations having 35, 45, and 60 degree angles.

5.4 Numerical Uncertainty

In Table 5.2 is the summary of the Grid Convergence Index (GCI) calculations for σ_o. Table 5.3 is the summary of the GCI calcuations for K_{run} and K_{branch}.

The numerical uncertainty for the head loss coefficients is low with a median of 0.65 percent error and a max of 3.7 percent. For the onset of cavitation parameter the median uncertainty is 1.2 percent with a max of 18.6 percent. This max uncertainty is not, in the author's estimation, representative of the actual uncertainty. This is because the GCI does not do well when the actual difference between solutions is small. For the case of where the GCI uncertainty is 18.6 percent the error between the mesh 1 and mesh 2 result was only 0.9 percent.

5.5 CFD Flow Visualization

Figures 5.8–5.21 illustrate the flow characteristics found in the CFD simulations and physical model test.

Table 5.2: Summary of GCI calculations for σ_O.

Simulation	N_1, N_2, N_3	r_{21}	r_{32}	ϕ_2	ϕ_2	ϕ_2	ϕ_{ext}^{21}	p	e_a^{21}	e_{ext}^{21}	GCI_{fine}^{21}
45° 4in 0%	3252707, 1429631, 627588	1.32	1.32	0.597	0.600	0.618	0.596	6.59	0.5%	0.1%	0.1%
45° 4in 40%		1.32	1.32	1.469	1.429	1.481	1.602	0.96	2.7%	8.3%	11.3%
45° 4in 100%		1.32	1.32	3.708	3.831	3.754	3.502	1.71	3.3%	5.9%	6.9%
45° 8ft 0%	4667700, 2034836, 919487	1.32	1.30	0.621	0.628	0.624	0.613	2.27	1.1%	1.3%	1.6%
45° 8ft 60%		1.32	1.30	2.602	2.569	2.530	2.733	0.81	1.3%	4.8%	6.3%
45° 8ft 100%		1.32	1.30	3.656	3.680	3.601	3.646	4.44	0.7%	0.3%	0.3%
35° 8ft 0%	5089675, 2232012, 1004689	1.32	1.30	0.676	0.688	0.715	0.668	3.19	1.8%	1.3%	1.6%
35° 8ft 60%		1.32	1.30	2.581	2.522	2.774	2.598	5.42	2.3%	0.7%	0.8%
35° 8ft 100%		1.32	1.30	2.810	2.852	2.989	2.792	4.47	1.5%	0.6%	0.8%
60° 8ft 0%	4313371, 1865389, 853074	1.32	1.30	0.559	0.552	0.704	0.559	12.1	1.2%	0.04%	0.1%
60° 8ft 60%		1.32	1.30	1.644	1.659	1.645	1.399	0.22	0.9%	17.5%	18.6%
60° 8ft 100%		1.32	1.30	4.635	4.672	4.911	4.630	7.22	0.8%	0.1%	0.2%
							Median:	3.82	1.2%	1.0%	1.2%
							Mean:	4.12	1.5%	3.4%	4.0%
							Standard Deviation:	3.40	0.9%	5.2%	5.8%
							Max:	12.1	3.3%	17.5%	18.6%
							Min:	0.22	0.5%	0.0%	0.1%

Figure 5.8 shows the pressure on the symmetry plane for $8ft$ diameter 45 degree angle bifurcation simulations at all flow splits. Figure 5.9 is the same as Figure 5.8 except zoomed into the crotch area. As the flow split percentage increases the maximum pressure increases. Figure 5.9 shows that the minimum and maximum pressures happen at the crotch.

Figure 5.10 shows a close up of the pressure on the symmetry plane and the wall around the crotch. The minimum pressure on the wall is the same as the symmetry plane and decreases as it gets farther from the wall. The max pressure on the wall follows the same trend as the minimum pressure except as it gets farther away from the wall the pressure decrease. This means that the lowest and highest pressures occur around the symmetry plane.

Figure 5.11 shows the velocity magnitude on the symmetry plane for $8ft$ diameter 45 degree angle bifurcation simulations at all flow splits. The maximum velocity increases with flow split percentage except at 100 percent where the maximum velocity is slightly lower then 80 percent. The maximum velocities in this figure are not the maximum velocities in the simulations, this is because there is an axial component that is not captured on the symmetry plane.

Table 5.3: Summary of GCI calculations for K_{run} and K_{branch}.

Through Run

Simulation	N_1, N_2, N_3	r_{21}	r_{32}	ϕ_2	ϕ_2	ϕ_2	ϕ_{ext}^{21}	p	e_a^{21}	e_{ext}^{21}	GCI_{fine}^{21}
45° 4in 0%	3252707, 1429631, 627588	1.32	1.32	0.232	0.234	0.233	0.229	2.20	1.1%	1.3%	1.7%
45° 4in 40%		1.32	1.32	0.107	0.107	0.102	0.108	7.88	0.5%	0.1%	0.1%
45° 4in 100%		1.32	1.32	0.393	0.391	0.377	0.393	6.76	0.6%	0.1%	0.1%
45° 8ft 0%	4667700, 2034836, 919487	1.32	1.30	0.158	0.160	0.159	0.155	1.67	1.3%	2.3%	2.8%
45° 8ft 60%		1.32	1.30	0.113	0.112	0.108	0.113	4.47	1.0%	0.4%	0.5%
45° 8ft 100%		1.32	1.30	0.352	0.348	0.334	0.353	5.29	1.0%	0.3%	0.4%
35° 8ft 0%	5089675, 2232012, 1004689	1.32	1.30	0.179	0.182	0.183	0.178	4.53	1.6%	0.6%	0.8%
35° 8ft 60%		1.32	1.30	0.113	0.112	0.108	0.114	4.08	1.2%	0.6%	0.7%
35° 8ft 100%		1.32	1.30	0.337	0.333	0.319	0.338	5.04	1.1%	0.4%	0.5%
60° 8ft 0%	4313371, 1865389, 853074	1.32	1.30	0.145	0.147	0.145	0.141	1.07	1.0%	3.0%	3.7%
60° 8ft 60%		1.32	1.30	0.111	0.112	0.105	0.111	7.57	0.9%	0.1%	0.1%
60° 8ft 100%		1.32	1.30	0.362	0.360	0.345	0.363	8.01	0.6%	0.1%	0.1%

Through Branch

45° 4in 0%	3252707, 1429631, 627588	1.32	1.32	0.991	0.988	0.978	0.991	5.39	0.2%	0.1%	0.1%
45° 4in 40%		1.32	1.32	0.614	0.609	0.597	0.617	3.52	0.8%	0.5%	0.6%
45° 4in 100%		1.32	1.32	0.528	0.524	0.517	0.532	2.40	0.7%	0.8%	1.0%
45° 8ft 0%	4667700, 2034836, 919487	1.32	1.30	0.963	0.959	0.947	0.964	4.93	0.3%	0.1%	0.2%
45° 8ft 60%		1.32	1.30	0.416	0.410	0.397	0.421	2.75	1.5%	1.3%	1.6%
45° 8ft 100%		1.32	1.30	0.430	0.428	0.417	0.430	7.22	0.4%	0.1%	0.1%
35° 8ft 0%	5089675, 2232012, 1004689	1.32	1.30	0.933	0.926	0.912	0.939	2.88	0.7%	0.6%	0.8%
35° 8ft 60%		1.32	1.30	0.344	0.337	0.325	0.354	1.99	2.1%	2.8%	3.6%
35° 8ft 100%		1.32	1.30	0.399	0.395	0.393	0.406	1.57	0.9%	1.7%	2.1%
60° 8ft 0%	4313371, 1865389, 853074	1.32	1.30	0.978	0.975	0.963	0.979	5.02	0.3%	0.1%	0.1%
60° 8ft 60%		1.32	1.30	0.551	0.545	0.529	0.555	3.55	1.2%	0.7%	0.9%
60° 8ft 100%		1.32	1.30	0.567	0.559	0.548	0.576	1.99	1.3%	1.7%	2.1%
							Median:	4.275	0.97%	0.55%	0.65%
							Mean:	4.24	0.9%	0.8%	1.0%
							Standard Deviation:	2.13	0.4%	0.9%	1.1%
							Max:	8.01	2.1%	3.0%	3.7%
							Min:	1.07	0.2%	0.1%	0.1%

Figure 5.12 shows streamlines on the symmetry plane for $8ft$ diameter, 45 degree angle bifurcation simulations at all flow splits. They are located in separated flow regions and recirculation regions. The separated flow regions and recirculation regions are very three dimensional as can be seen in Figures 5.15–5.21. Figure 5.12 shows the relative size and location of each separation and recirculation region at each flow split. Figure 5.13 shows streamlines on the symmetry plane for $8ft$ diameter 35 and 60 degree angle bifurcation simulations at 60 percent flow split. These are for comparison with the 60 percent flow split in Figure 5.12(d). The 45 and 60 degree angles show about the same flow separation and the 35 degree angle has less of a separation region.

Figure 5.14 show the stagnation region that occurs at the crotch for most of the flow conditions. The velocity has to increase from this stagnation region to get around the corner at the crotch, causing the pressure to drop dramatically this area.

Figures 5.15–5.17 show streamlines for $8ft$ diameter, 45 degree angle bifurcation simulations at 0, 60, and 100 percent flow splits, respectively. These are shown to illustrate the general flow pattern at the flow splits.

Figure 5.18 and 5.19 are for comparison of the separation regions in the branch of the physical test and the CFD with 50-60 percent flow through the branch, they are almost identical. Figure 5.20 and 5.21 are for comparison of the separation regions in the branch of the physical test and the CFD with 100 percent flow through the branch, they are almost identical.

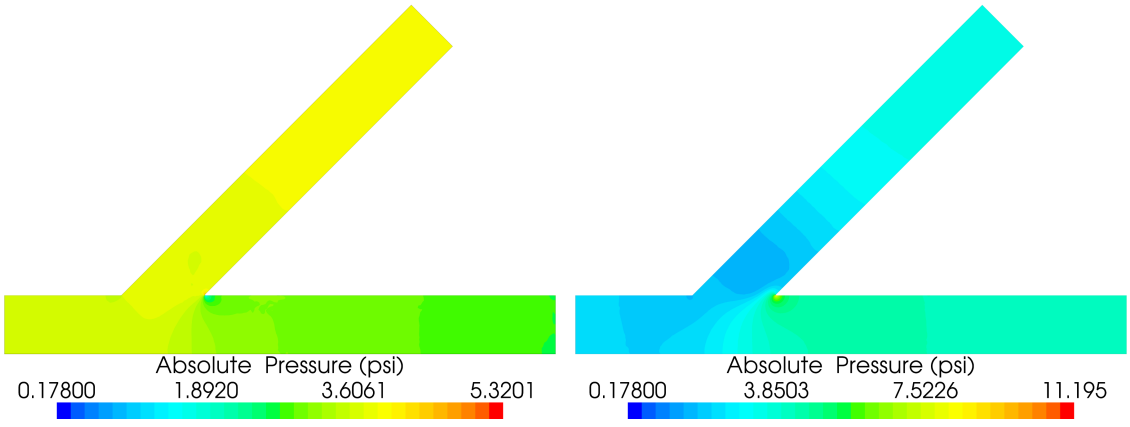

(a) 0 percent flow split (b) 20 percent flow split

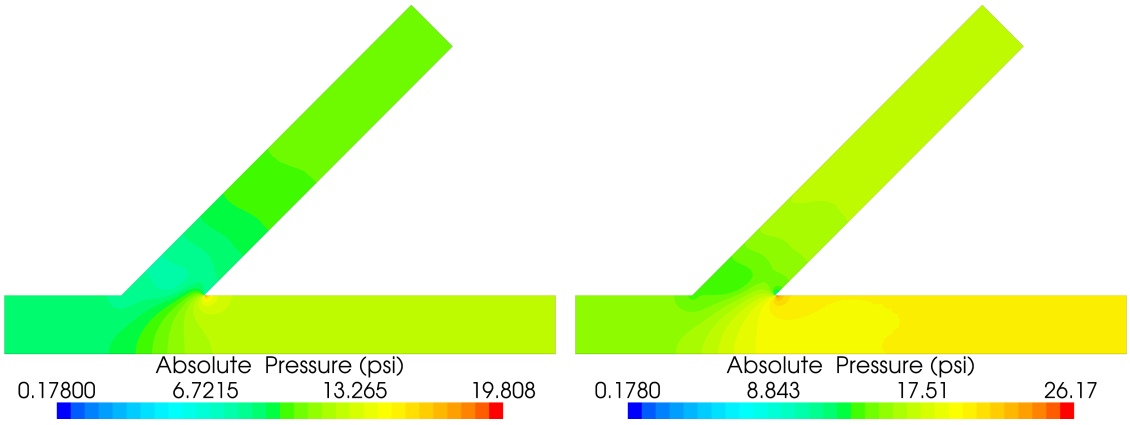

(c) 40 percent flow split (d) 60 percent flow split

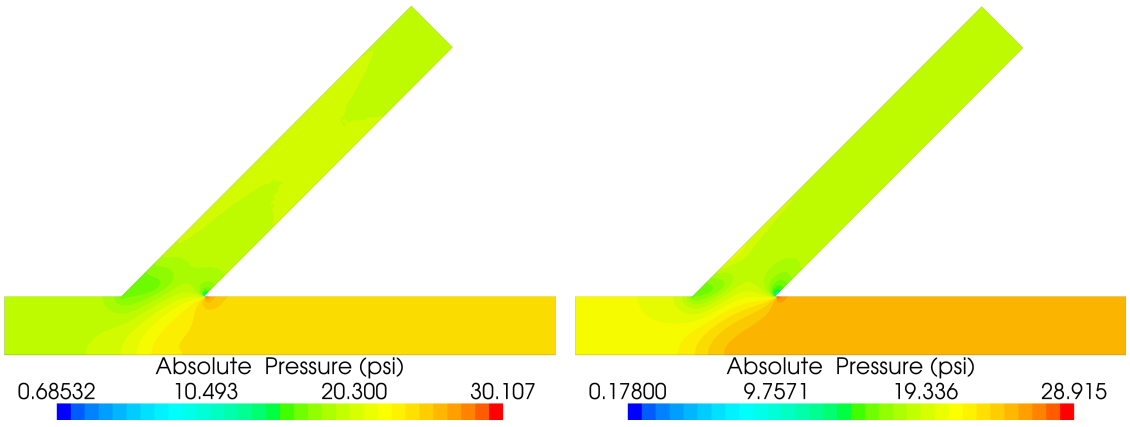

(e) 80 percent flow split (f) 100 percent flow split

Fig. 5.8: Pressure on symmetry plane for 45 degree angle 8ft diameter bifurcation.

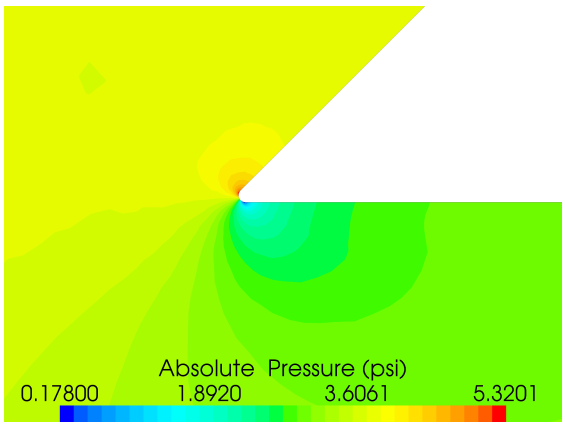

(a) 0 percent flow split

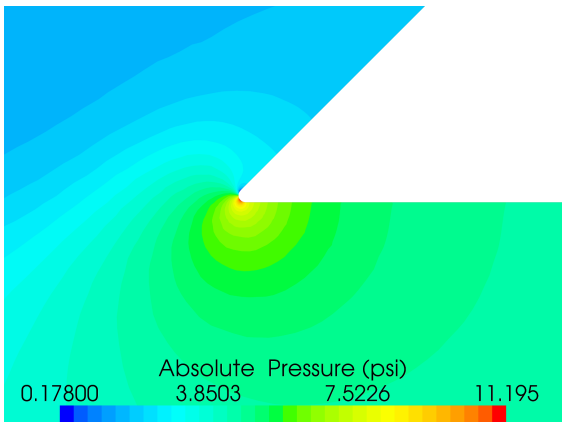

(b) 20 percent flow split

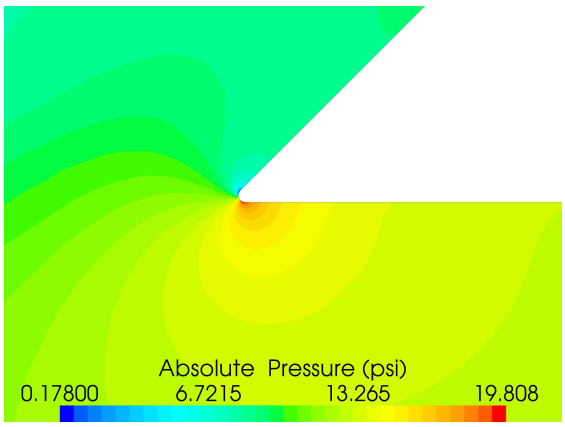

(c) 40 percent flow split

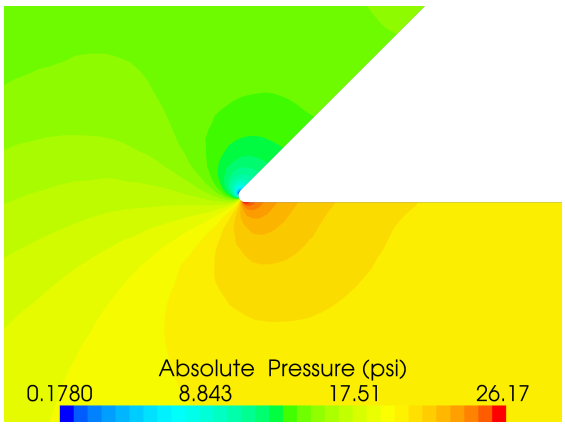

(d) 60 percent flow split

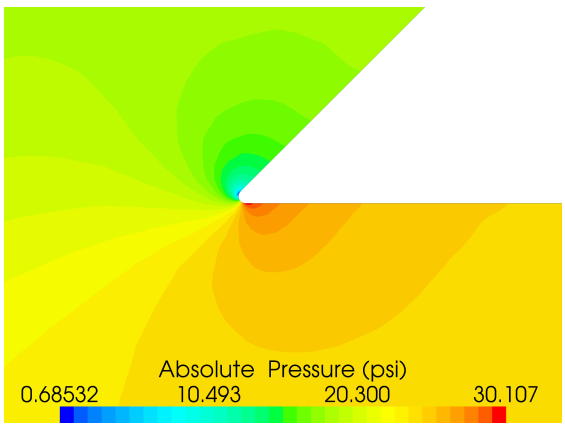

(e) 80 percent flow split

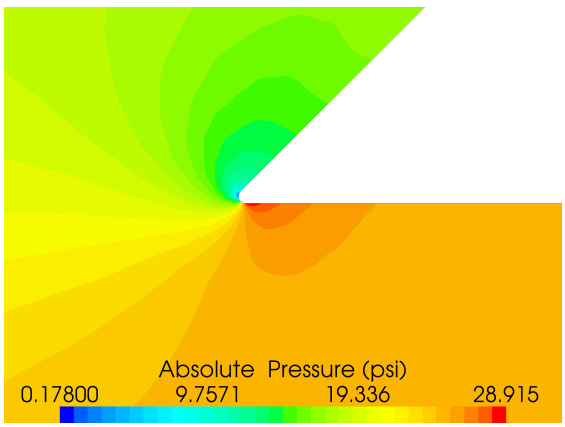

(f) 100 percent flow split

Fig. 5.9: Pressure on symmetry plane for 45 degree angle $8ft$ diameter bifurcation, zoomed into crotch area.

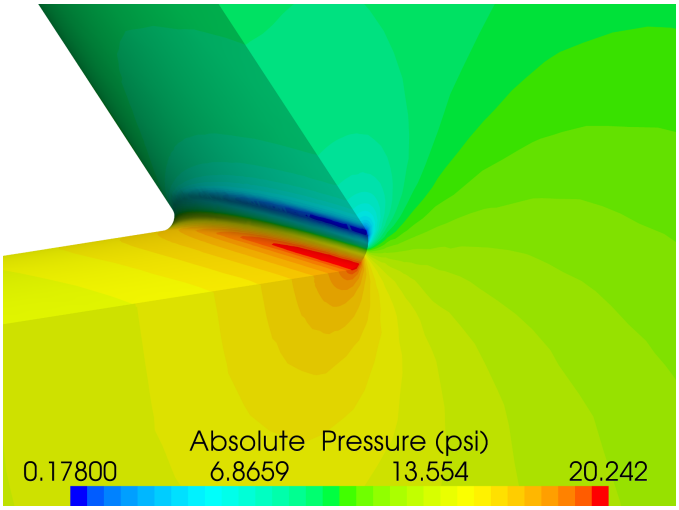

Fig. 5.10: Pressure on symmetry plane and wall for 45 degree angle 8ft diameter bifurcation with a 40 percent flow split.

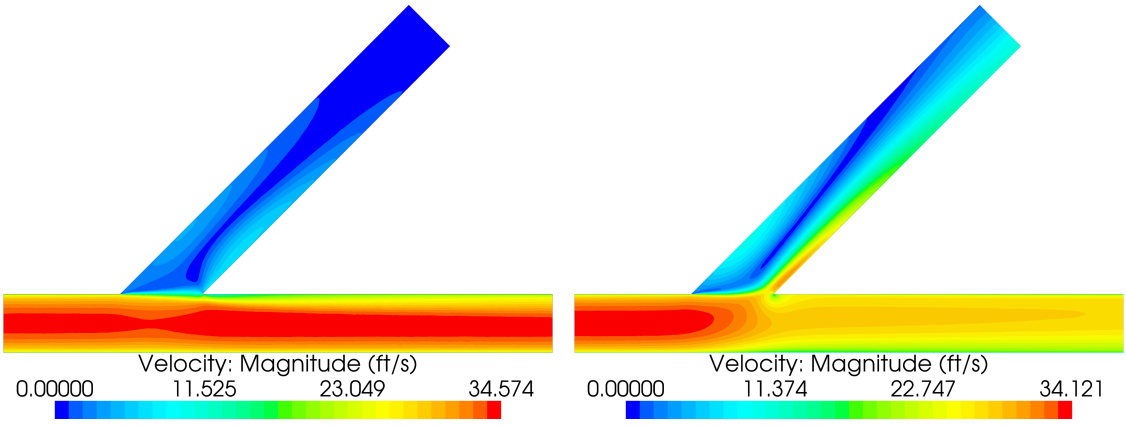

(a) 0 percent flow split

(b) 20 percent flow split

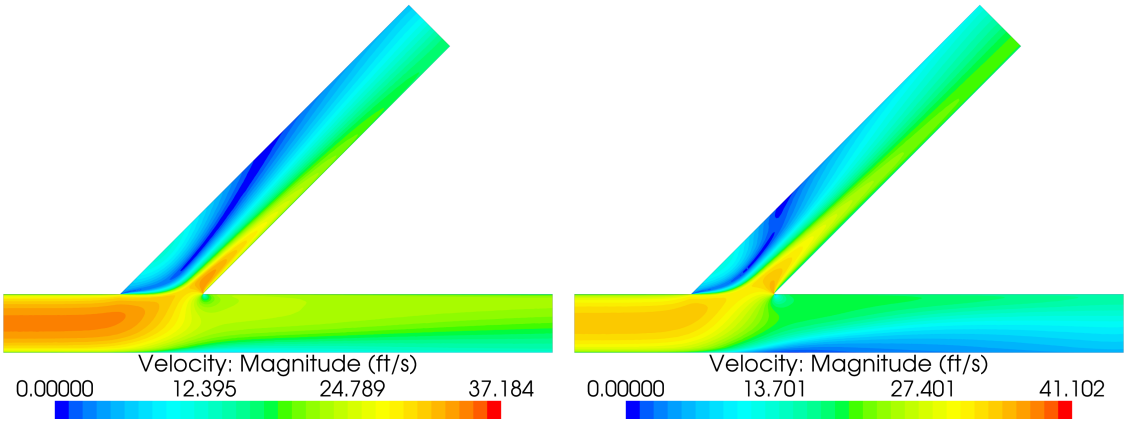

(c) 40 percent flow split

(d) 60 percent flow split

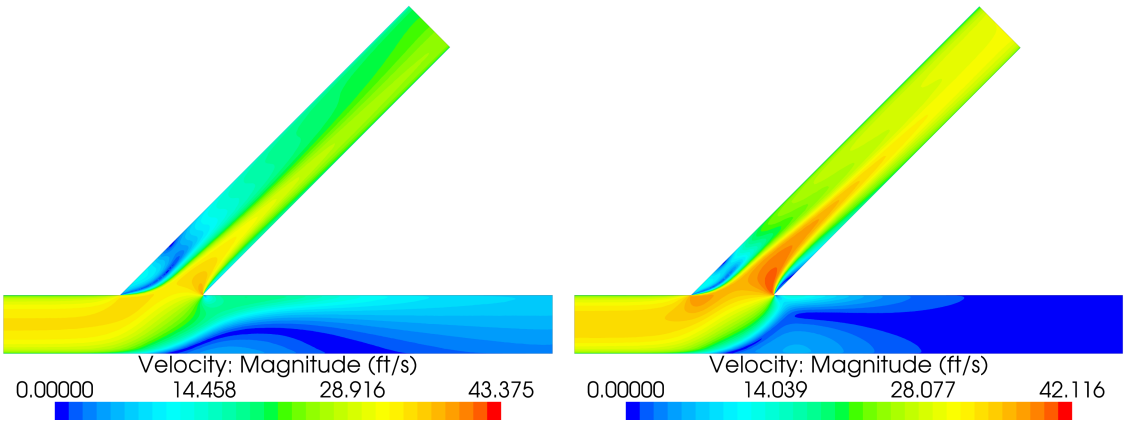

(e) 80 percent flow split

(f) 100 percent flow split

Fig. 5.11: Velocity magnitude on symmetry plane for 45 degree angle $8ft$ diameter bifurcation.

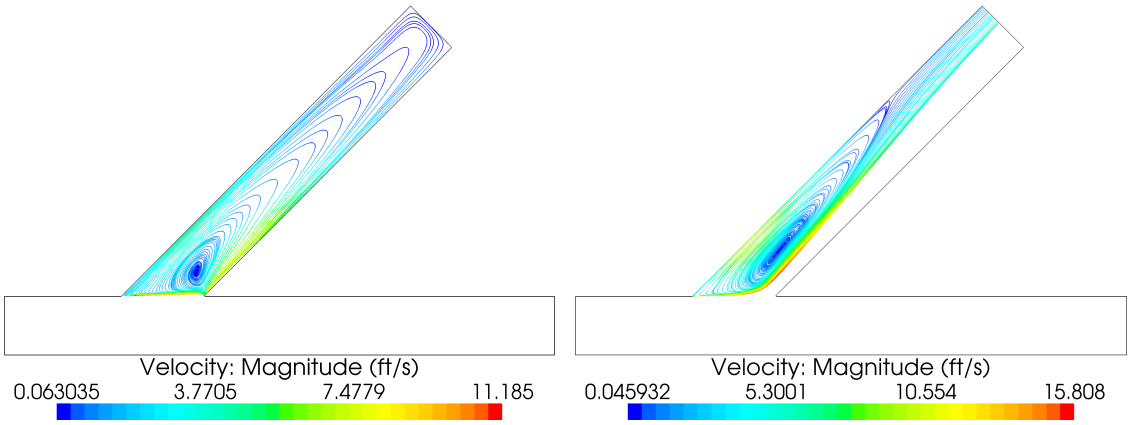

(a) 0 percent flow split

(b) 20 percent flow split

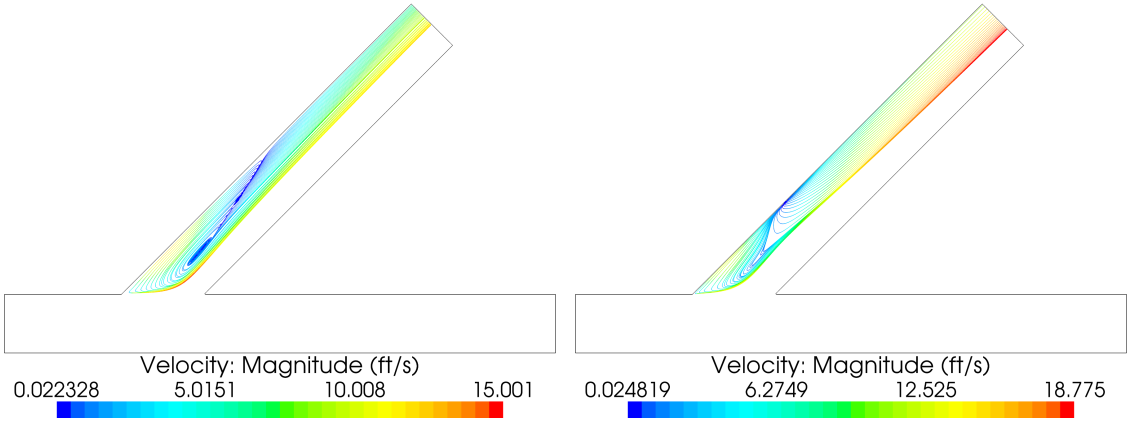

(c) 40 percent flow split

(d) 60 percent flow split

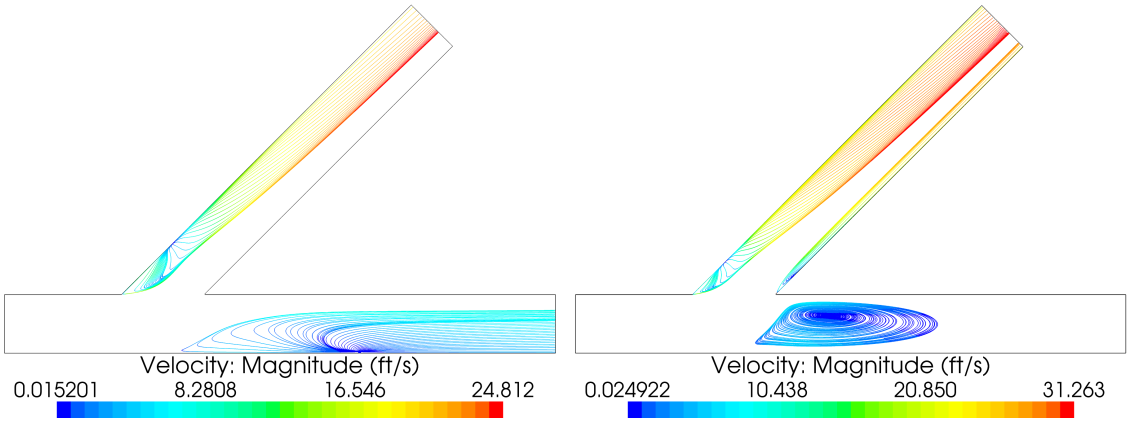

(e) 80 percent flow split

(f) 100 percent flow split

Fig. 5.12: Constrained streamline on the symmetry plane in recirculation zone and separation region for 45 degree angle 8ft diameter bifurcation.

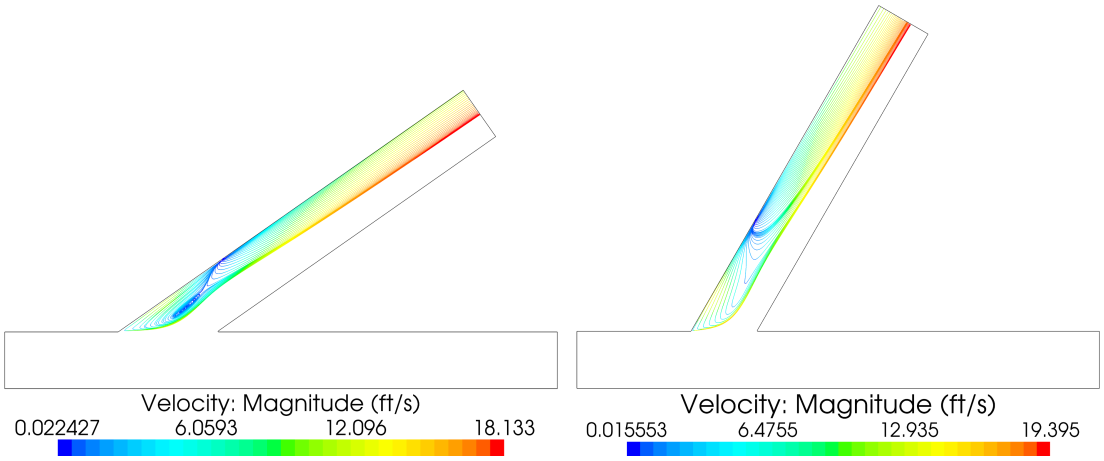

(a) 60 percent flow split (b) 60 percent flow split

Fig. 5.13: Constrained streamline on the symmetry plane in recirculation zone and separation region for 35 and 60 degree angle $8ft$ diameter bifurcation.

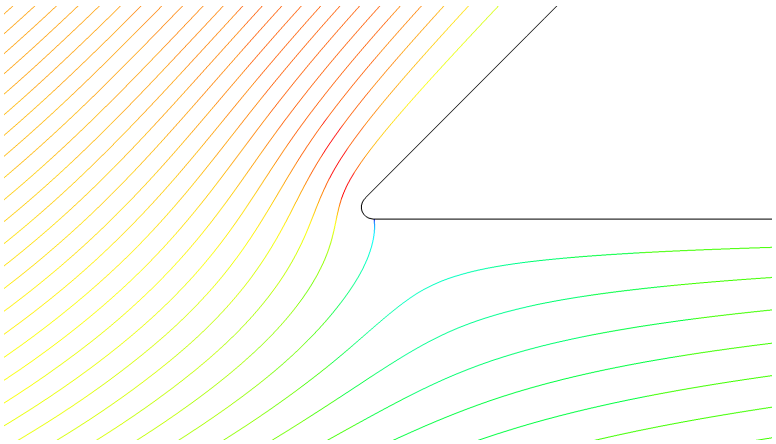

Fig. 5.14: Streamlines showing the stagnation region in a 45 degree angle, $8ft$ diameter bifurcation with a 60 percent flow split.

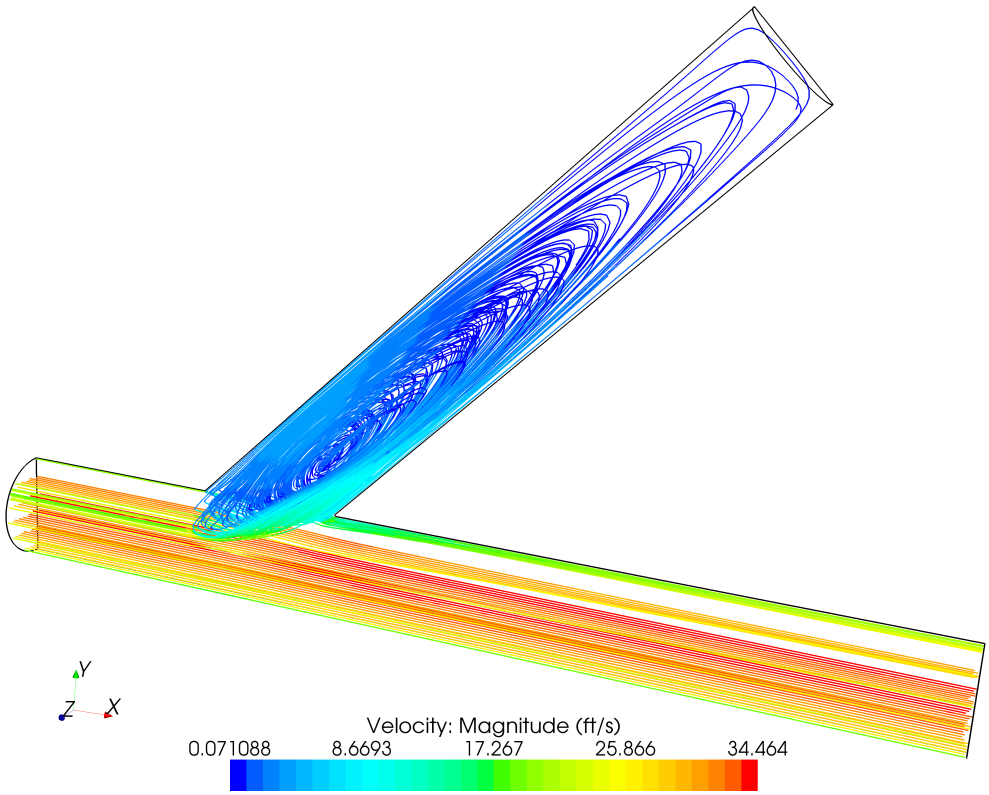

Fig. 5.15: Streamlines in 45 degree angle $8ft$ diameter bifurcation with a 0 percent flow split.

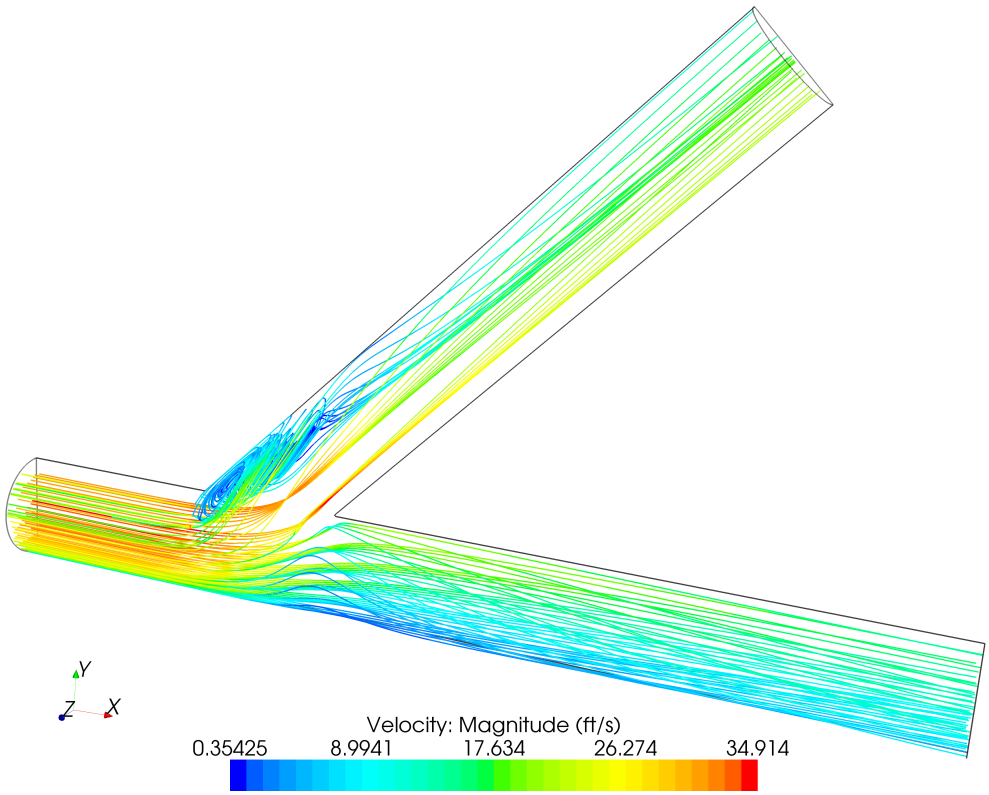

Fig. 5.16: Streamlines in 45 degree angle $8\,ft$ diameter bifurcation with a 60 percent flow split.

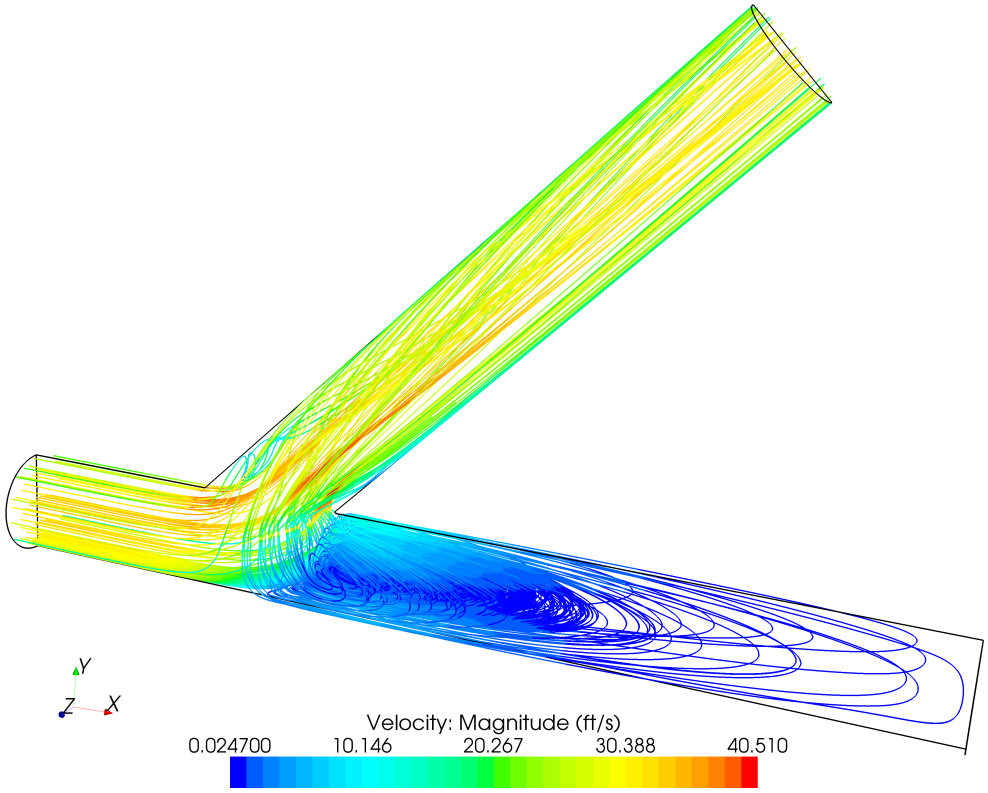

Fig. 5.17: Streamlines in 45 degree angle $8ft$ diameter bifurcation with a 100 percent flow split.

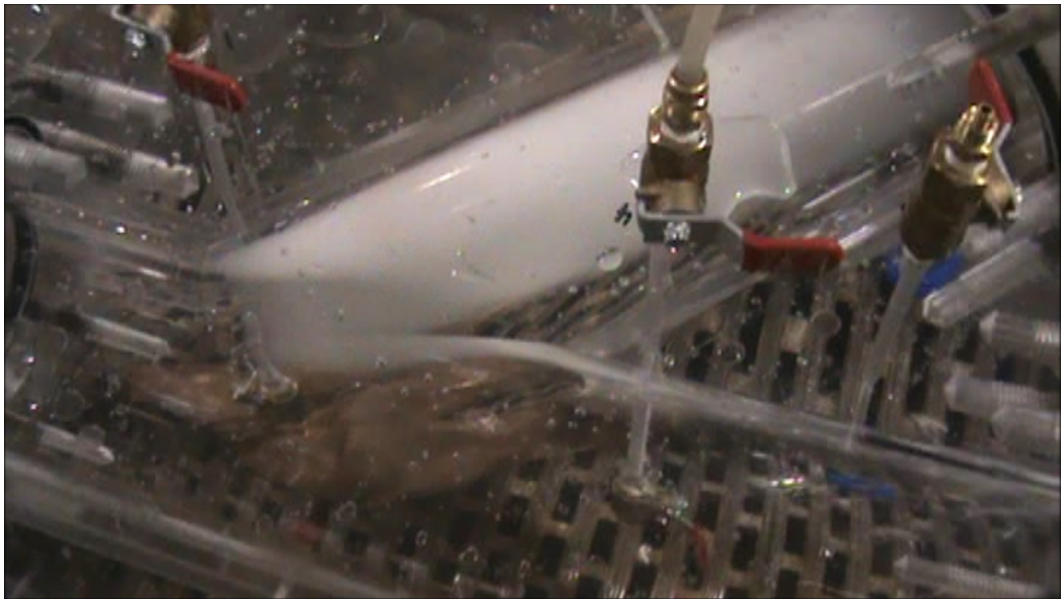

Fig. 5.18: Physical test flow visualization of separation region with 50 percent flow through the branch, obtained by inserting air in branch with air compressor.

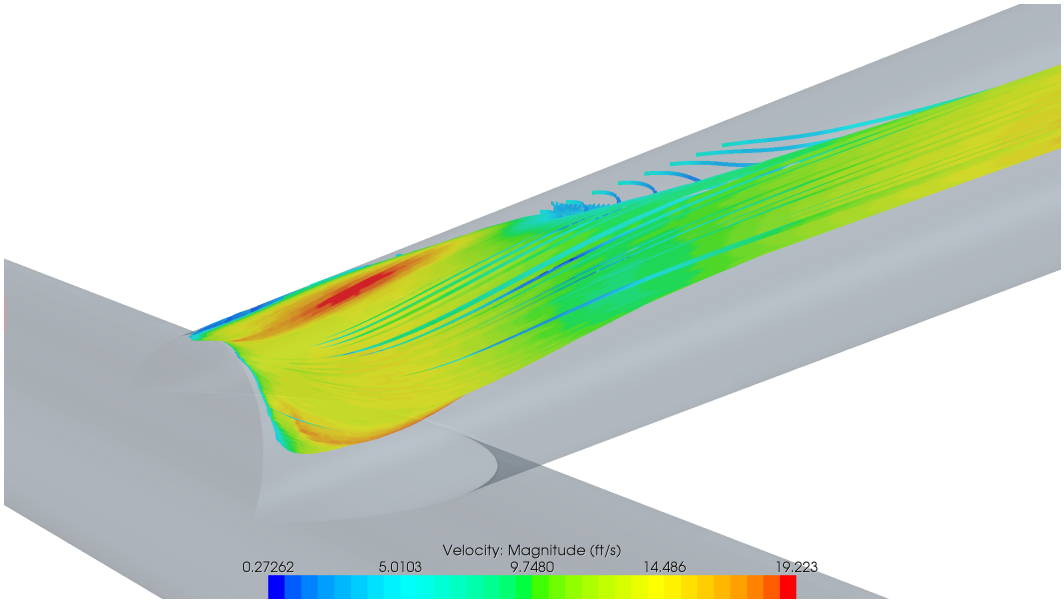

Fig. 5.19: CFD flow visualization of separation region with 60 percent flow through the branch using streamlines.

Fig. 5.20: Physical test flow visualization of separation region with 100 percent flow through the branch, obtained by inserting air in branch with air compressor.

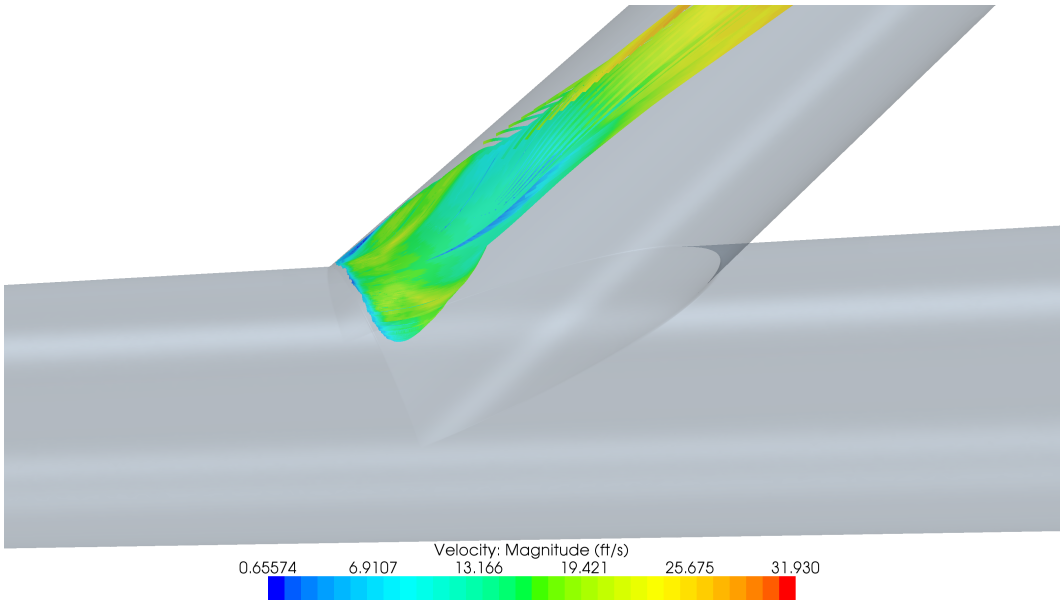

Fig. 5.21: CFD flow visualization of separation region with 100 percent flow through the branch using streamlines.

Chapter 6

Discussion and Conclusion

6.1 Cavitation

By only considering the pressure the CFD simulations showed little scale effect for σ_o. For a comparison, valves have a log scale effect from one size diameter to another with an exponential scaling factor (Y). Y is used to scale the ratios of the diameter to extrapolate data from one size of valve to another size, for valves $Y = 0.3K^{-0.25}$ [4]. If we take $K = 1$ for a valve then Y=0.3, and this results in a significant scaling effect. However, for diameters larger than 3 ft the relation brakes down and there is little to no scale effect on σ_o [2]. For this study the log scaling effect was noted, but to an almost insignificant degree. Y factors from the CFD were either zero, at 0 and 100 percent flow splits, or had an average of 0.05, for the 20 to 80 percent flow splits. These are dramatically different from the valve scaling effects, and show that there are negligible scale effects associated with nonsymmetric bifurcations.

One limitation of the CFD analysis is that the model did not take into account that cavitation more easily occurs as the geometry increases in size due to the increase in the number of nuclei. The author suspects that this effect could cause the recommended σ_o lines in Figures 5.2-5.5 to be lower than they should be, however without any data on nuclei effects for nonsymmetric bifurcations available and the fact that incipient and constant cavitation scaling effects stop at about $3ft$ diameter for valves, the recommended σ_o lines are, in the author's judgment, conservative. If desired, a safety factor could be added to the recommended σ_o lines to help negate this uncertainty.

6.2 Head Loss Coefficient

The CFD shows that K_{run} and K_{branch} are not independent of Reynolds Number. The effects of the Reynolds Number seem to also follow a log scale and should be accounted for when extrapolating data from one flow condition to another. AWWA [21] reported a K_{branch} for a 45 degree angle

bifurcation with 100 percent flow through the branch should be about 1.25. This was the only loss coefficient data that could be found for nonsymmetric bifurcations. That result may be contrasted to values on the order of 0.5 as shown in Figure 5.6. Nonsymmetric bifurcations have not attracted much attention relative to other pipe fittings and pipe geometries with regard to loss coefficient data. This study has, in part, remedied this lack of data.

6.3 Example Problem

To help illustrate how the cavitation results can be used an example problem is given as follows:

Setup: An operator of a hydroelectric facility has to do an emergency evacuation through the outlet works piping, but would also like to keep diverting water through the branch to the turbines for continued electric generation. However, he is unsure if diverting the water through the branch will cause cavitation.

Given: The turbine capacity is $1200 cfs$ and the evacuation flow is $2000 cfs$. The pressure just upstream of the bifurcation is calculated to be $10 psig$ and the vapor pressure is $-11.8 psig$. The diameter of piping is $8 ft$ and the bifurcation angle is 35 degrees.

Solution: The velocity is easily determined to be $39.8 ft/s$ and the flow split through the branch to be 60 percent. Now using this information in Eq. 1.1 (making sure to take care of unit conversions) it is determined that σ for this operating condition would be 2.0. Figure 5.4 indicates that to have a safe operating condition σ should be above 2.6. Therefore, one would expect cavitation to occur at the bifurcation under these conditions. The upstream pressure does not change for different flow splits so from Figure 5.4 shows that at about 33 percent flow though the branch, σ_o drops below 2. Using this flow split there would be $660 cfs$ going to the turbines. This is 55 percent less than full capacity, but cavitation will not develop beyond the onset at the bifurcation and no cavitation damage would be expected.

6.4 Future Research

This study only utilized pressure as an indicator to predict the onset of cavitation. STAR-CCM+ comes with a cavitation model that uses the volume of fluid method for simulating cavitation. This could be used to match to physical test results and then use the same parameters that matched

the physical test results on the larger diameter. This would take into account the nuclei effect that was not able to be analyzed in the present study. This approach would be very tedious and require significantly more computational time then was needed in this study, but could potentially give better results.

Further validation could potentially be carried out at existing dam bifurcations under the right conditions. These conditions would be rare and the owners of the dam would have to agree to such a test, but this would give actual points that could be used for further analysis.

6.5 Extension of Analysis Method to Other Geometries

The CFD approach used in this study for finding the onset of cavitation should be used with caution for other pipe fittings or geometries. Using steady state pressures CFD results without physical validation could lead to erroneous results. The results from this study and from Glenn [7] are a prime examples of how some results are not physically meaningful. These discrepancies would not have been found in this study without the physical test.

6.6 Conclusion

The objective of this study was to find the conditions for the onset of cavitation and head loss coefficients for nonsymmetric bifurcations. This was done using a combination of physical model testing and CFD simulations. Using both a physical model and CFD together gave greater insight and better results then only using one or the other by itself. Using both physical and CFD results allowed the extension of the model test to be extrapolated to larger more regularly seen bifurcation sizes. This was done without the huge expense that would be required to do a full scale testing.

The results presented in this study should be of great value to designers and operators of systems that include nonsymmetric bifurcations. Although this study was not exhaustive, it presents valuable data that was not previously found in the literature. The results of this study provide insight into operating conditions to avoid cavitation damage for nonsymmetric bifurcations.

Bibliography

[1] Knapp, R. T., Daily, J. W., and Hammitt, F. G., *Cavitation*, McGraw-Hill, Englewood Cliffs, NJ, 1970.

[2] Tullis, J. P., *Cavitation Guide for Control Valves*, Division of Engineering Office of Nuclear Regulatory Research, Washington, DC, 1993.

[3] Joseph, D. D., "Cavitation and the State of Stress in Flowing Liquid," *Journal of Fluid Mechanics*, Vol. 366, 1998, pp. 367–378.

[4] America Water Works Association, *Butterfly Valves: Torque, Head Loss, and Cavitation Analysis, Manual of Water Supply Practices, M49*, AWWA, Denver, CO, 2012.

[5] Finnemore, E. J., and Franzini, J. B., *Fluid Mechanics with Engineering Applications*, McGraw-Hill, New York, 2006.

[6] Tullis, J. P., *Hydraulics of Pipelines-Pumps, Valves, Cavitation, Transients*, Wiley and Sons, New York, 1989.

[7] Glenn, A. H., and Decker, G., "Using Computational Fluid Dynamics to Predict the Onset of Cavitation," *Valve World 2008 Conference, Maastricht, the Netherlands*, 2008, [http://www.valve-world.net/pdf/vw08ce_control_flowserveIIpdf.pdf?resourceId=82 Accessed 3/10/13].

[8] Feng, W., "Numerical Simulation of the Flow Field to the Double Eccentric Butterfly Valve and Performance Prediction," *Power and Energy Engineering Conference*, 2009, pp. 1–4.

[9] Sadrnezhad, S. A., "Hydrolic Model Studies of Non-Symmetric Y-Branches in Karun-I," *Department of Civil Engeering, K. N. Toosi University of Technolagy Teheran*, 2002.

[10] The American Iron and Steel Institute, "Buried Steel Penstocks," *Steel Plate Engineering Data-Volume 4*, 1992.

[11] Hollingshead, C. L., "Discharge Coefficeint Performace of Ventri, Standard Concentric Orfice Plate, V-Cone, and Wdge Flow meters at Small Renolds Numbers," Masters thesis, Utah State University, Logan, UT, 2011.

[12] Del Toro, A., "Computational Fluid Dynamics Analysis of Butterfly Valve Performance Factors," Masters thesis, Utah State University, Logan, UT, 2012.

[13] Sibilla, S., "Hydrodynamic Characterization of a Nozzle Check Valve by Numerical Simulation," *Journal of Fluids Engineering*, Vol. 130, 2008.

[14] Instrument Society of America (ISA), *Control Valve Capacity Test Procedure An American National Standard. ANSI/ISA-S75.02-1988*, Instrument Society of America, Research Triangle Park, NC, 1988.

[15] American Society of Mechanical Engineers (ASME), *Test Uncertainty An American National Standard*, ASME PTC 19.1-2005, 2006.

[16] CD-Adapco, STAR-CCM+ version 7.04, Users Manual.

[17] Davidson, L., Nielsen, P. V., and Sveningsson, A., "Modications of the V2-F Model for Computing the Flow in a 3D Wall Jet," *Turbulence, Heat and Mass Transfer*, Vol. 4, 2003, pp. 8577–584.

[18] Durbine, P. A., "On the k-e Stagnation Point Anomaly," *International Journal of Heat and Fluid Flow*, Vol. 17, 1996, pp. 89–90.

[19] Lien, S. L., Kaltitzin, G., and Durbin, P. A., "RANS Modeling for Compressible and Transitional Flows," *Center for Turbulence Research - Proceedings of the Summer Program*, 2008.

[20] Celik, I., Ghia, U., Roache, P., Freitas, C., Coleman, H., and Raad, P., "Procedure for Estimation and Reporting of Uncertainty Due to Discretization in CFD Applications," *Journal of Fluid Mechanics*, Vol. 130, No. 7, 2008.

[21] America Water Works Association, *Steel Pipe-A Guide for Design and Installation, Manual of Water Supply Practices, M11*, AWWA, Denver, CO, 1989.

Appendices

Appendix A

Prism Layer Calculator

Prism Layer Calculator

by Steven Daniels

T = Total Thickness of the layers

N = Number of prism layers

gr = Growth rate or "prism layer stretch"

t_1 = the thickness of the first layer

t_N = the thickness of the last layer

note: before using answers check make sure number next to each other match

There are three varations of inputs depending on what you want.

The last two varations are the most useful, with the middle one having the same inputs as Star-CCM+.

Needed Functions:

$$f(t_1) := \sum_{n=1}^{N} \left(t_1 \cdot (gr)^{(n-1)} \right) - T$$

$$f2(gr) := \sum_{n=1}^{N} \left(t_1 \cdot (gr)^{(n-1)} \right) - T$$

Inputs: $t_1 := 1.5 \cdot 10^{-5}$ $N := 78$ $gr := 1.114$

$$T := \sum_{n=1}^{N} \left(t_1 \cdot (gr)^{(n-1)} \right) \qquad t_N := t_1 \cdot gr^{(N-1)}$$

Results: $T = 0.597221756569771$ $t_N = 0.0611295154838$

Inputs: $T := .6$ $N := 78$ $gr := 1.114$

$t_{12} := 5 \cdot 10^{-5}$ $t_{13} := 4 \cdot 10^{-5}$

for $i \in 1..1000$

$t_1 := t_{12} - \dfrac{f(t_{12}) \cdot (t_{13} - t_{12})}{f(t_{13}) - f(t_{12})}$

$t_{13} := t_{12}$

$t_{12} := t_1$

$t_N := t_1 \cdot gr^{(N-1)}$

Results: $t_1 = 1.5069779192 \cdot 10^{-5}$ $t_N = 0.0614138867$

$t_{13} = 1.5069779192 \cdot 10^{-5}$

Inputs: $T := .6$ $N := 78$ $t_1 := 1.5 \cdot 10^{-5}$

$gr_2 := 1.2$ $gr_3 := 1.3$

for $i \in 1..10000$

$gr_1 := gr_2 - \dfrac{f2(gr_2) \cdot (gr_3 - gr_2)}{f2(gr_3) - f2(gr_2)}$

$gr_3 := gr_2$

$gr_2 := gr_1$

$t_N := t_1 \cdot gr_1^{(N-1)}$

Results: $gr_1 = 1.1140757593$ $t_N = 0.0614138867$

$gr_3 = 1.1140757593$

Appendix B

CAD Model

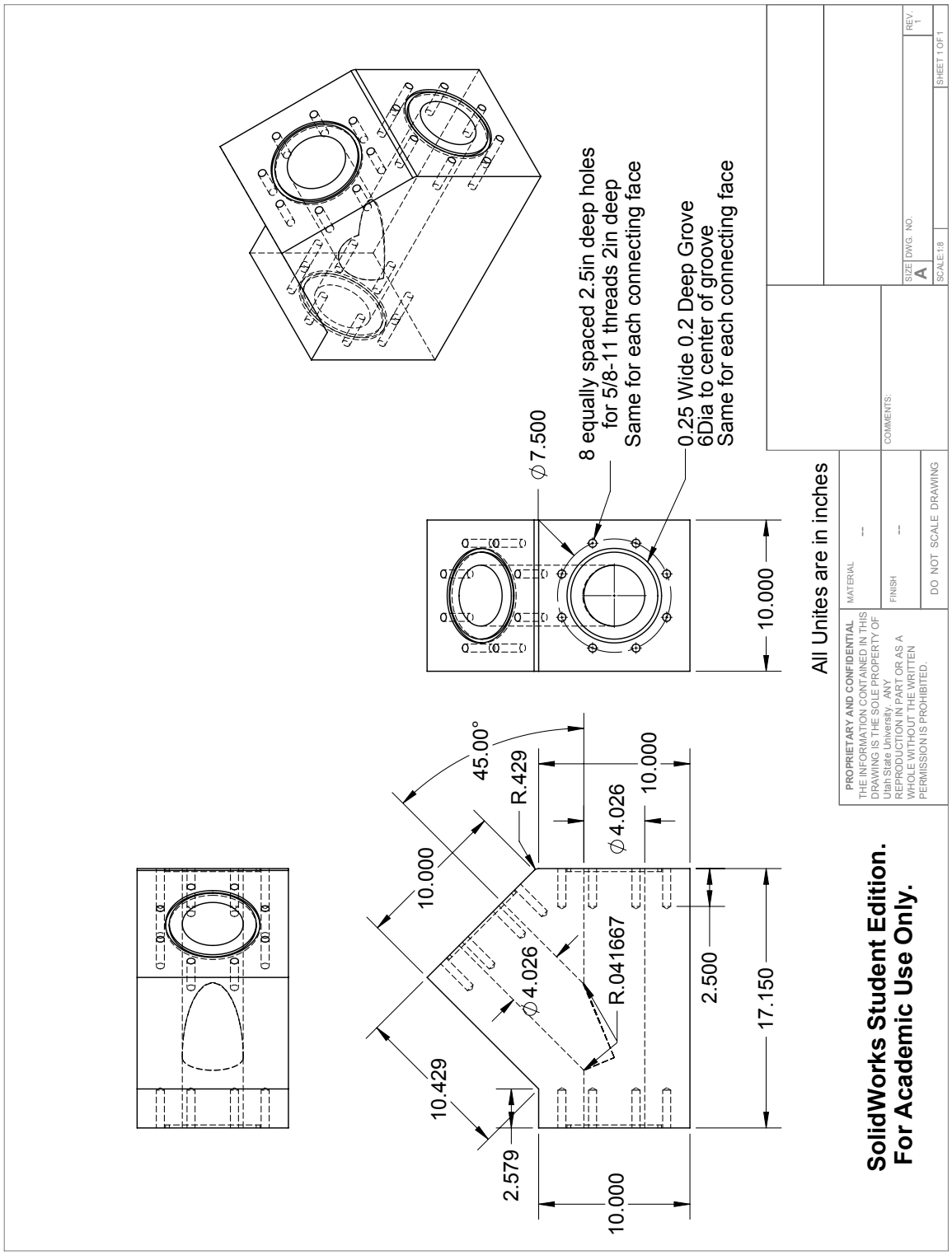

Fig. B.1: Technical drawing of bifurcation test model.

Appendix C

CFD Uncertainty

What follows is the SMath Studio print out of the calculation tabulated in Table 5.2 and 5.3.

Grid Convergence Index(GCI) Calculations

These calcuation were done in SMath Studio.
The first GCI calcuations are all shown.
The ones that follow after show just the results.

GCI for Onset of Cavitation:

45 Degree, 4inch Diameter Bifurcations with 0% Split and Velocity of 45 ft/s

Number of cells and associated φ:

$N1 = 3252707$ $N2 = 1429631$ $N3 = 627588$

$\varphi_1 = 0.5965183$ $\varphi_2 = 0.5995322$ $\varphi_3 = 0.6179311$

Calculations:

Ratios:

$$r_{21} = \left(\frac{N1}{N2}\right)^{\frac{1}{3}} \qquad r_{32} = \left(\frac{N2}{N3}\right)^{\frac{1}{3}}$$

Apparent Order:

$\varepsilon_{32} = \varphi_3 - \varphi_2$ $\varepsilon_{21} = \varphi_2 - \varphi_1$

$$s = \operatorname{sign}\left(\frac{\varepsilon_{32}}{\varepsilon_{21}}\right) \qquad p = \frac{1}{\ln(r_{21})} \cdot \left| \ln\left(\left|\frac{\varepsilon_{32}}{\varepsilon_{21}}\right|\right) + 0 \right| \qquad p_{old} = 0$$

while $\left|p_{old} - p\right| \geq 10^{-10}$

$p_{old} = p$

$$q = \ln\left(\frac{r_{21}^{\,p} - s}{r_{32}^{\,p} - s}\right)$$

$$p = \frac{1}{\ln(r_{21})} \cdot \left| \ln\left(\left|\frac{\varepsilon_{32}}{\varepsilon_{21}}\right|\right) + q \right|$$

$p = 6.590154937127$

$p_{old} = 6.5901549371096$

Extrapolated Values:

$$\varphi_{ext21} = \frac{r_{21}^{p} \cdot \varphi_1 - \varphi_2}{r_{21}^{p} - 1} \qquad \varphi_{ext32} = \frac{r_{32}^{p} \cdot \varphi_2 - \varphi_3}{r_{32}^{p} - 1}$$

Errors:

$$e_{a21} = \left| \frac{\varphi_1 - \varphi_2}{\varphi_1} \right| \cdot 100 \qquad e_{ext21} = \left| \frac{\varphi_{ext21} - \varphi_1}{\varphi_{ext21}} \right| \cdot 100$$

$$GCI_{fine} = \frac{1.25 \cdot e_{a21}}{r_{21}^{p} - 1}$$

$GCI_{fine} = 0.12\%$

$r_{21} = 1.32$ $\varphi_{ext21} = 0.5959$

$r_{32} = 1.32$ $e_{a21} = 0.51\%$

$p = 6.59$ $e_{ext21} = 0.1\%$

45 Degree, 4inch Diameter Bifurcations with 40% Split and Velocity of 45ft/s

$\varphi_1 = 1.469256$ $\varphi_2 = 1.429299$ $\varphi_3 = 1.481317$

$GCI_{fine} = 11.3\%$

$p = 0.96$ $\varphi_{ext21} = 1.6018$

$r_{21} = 1.32$ $e_{a21} = 2.72\%$

$r_{32} = 1.32$ $e_{ext21} = 8.3\%$

45 Degree, 4inch Diameter Bifurcations with 100% Split and Velocity of 45ft/s

$\varphi_1 = 3.707838$ $\varphi_2 = 3.831024$ $\varphi_3 = 3.753912$

$GCI_{fine} = 6.9\%$

$p = 1.71$ $\varphi_{ext21} = 3.5019$

$r_{21} = 1.32$ $e_{a21} = 3.32\%$

$r_{32} = 1.32$ $e_{ext21} = 5.9\%$

45 Degree, 8ft Diameter Bifurcations with 0% Split and Velocity of 30ft/s

Number of cells and associated φ:

$N1 = 4667700$ $N2 = 2034836$ $N3 = 919487$

$\varphi_1 = 0.6209228$ $\varphi_2 = 0.6277463$ $\varphi_3 = 0.6241645$

$GCI_{fine} = 1.6\%$ $p = 2.27$ $\varphi_{ext21} = 0.6131$

$r_{21} = 1.32$ $e_{a21} = 1.1\%$

$r_{32} = 1.3$ $e_{ext21} = 1.3\%$

45 Degree, 8ft Diameter Bifurcations with 60% Split and Velocity of 30ft/s

$\varphi_1 = 2.602271$ $\varphi_2 = 2.569365$ $\varphi_3 = 2.530162$

$GCI_{fine} = 6.3\%$ $p = 0.81$ $\varphi_{ext21} = 2.7331$

$r_{21} = 1.32$ $e_{a21} = 1.26\%$

$r_{32} = 1.3$ $e_{ext21} = 4.8\%$

45 Degree, 8ft Diameter Bifurcations with 100% Split and Velocity of 30ft/s

$\varphi_1 = 3.655666$ $\varphi_2 = 3.679688$ $\varphi_3 = 3.600875$

$GCI_{fine} = 0.34\%$ $p = 4.44$ $\varphi_{ext21} = 3.6457$

$r_{21} = 1.32$ $e_{a21} = 0.66\%$

$r_{32} = 1.3$ $e_{ext21} = 0.3\%$

35 Degree, 8ft Diameter Bifurcations with 0% Split and Velocity of 30ft/s

Number of cells and associated φ:

$N1 = 5089675$ $N2 = 2232012$ $N3 = 1004689$

$\varphi_1 = 0.6761323$ $\varphi_2 = 0.6879565$ $\varphi_3 = 0.7150632$

$GCI_{fine} = 1.6\%$ $p = 3.19$ $\varphi_{ext21} = 0.6677$

$r_{21} = 1.32$ $e_{a21} = 1.75\%$

$r_{32} = 1.3$ $e_{ext21} = 1.3\%$

35 Degree, 8ft Diameter Bifurcations with 60% Split and Velocity of 30ft/s

$\varphi_1 = 2.581142$ $\varphi_2 = 2.522051$ $\varphi_3 = 2.774357$

$GCI_{fine} = 0.8\%$ $p = 5.42$ $r_{21} = 1.32$ $r_{32} = 1.3$ $\varphi_{ext21} = 2.5983$ $e_{a21} = 2.29\%$ $e_{ext21} = 0.7\%$

35 Degree, 8ft Diameter Bifurcations with 100% Split and Velocity of 30ft/s

$\varphi_1 = 2.809611$ $\varphi_2 = 2.851941$ $\varphi_3 = 2.988645$

$GCI_{fine} = 0.78\%$ $p = 4.47$ $r_{21} = 1.32$ $r_{32} = 1.3$ $\varphi_{ext21} = 2.7921$ $e_{a21} = 1.51\%$ $e_{ext21} = 0.6\%$

60 Degree, 8ft Diameter Bifurcations with 0% Split and Velocity of 30ft/s

Number of cells and associated φ:

$N1 = 4313371$ $N2 = 1865389$ $N3 = 853074$

$\varphi_1 = 0.558579$ $\varphi_2 = 0.5521414$ $\varphi_3 = 0.704168$

$GCI_{fine} = 0.1\%$ $p = 12.09$ $r_{21} = 1.32$ $r_{32} = 1.3$ $\varphi_{ext21} = 0.5588$ $e_{a21} = 1.15\%$ $e_{ext21} = 0.04\%$

60 Degree, 8ft Diameter Bifurcations with 60% Split and Velocity of 30ft/s

$\varphi_1 = 1.643729$ $\varphi_2 = 1.658884$ $\varphi_3 = 1.644643$

$GCI_{fine} = 18.6\%$ $p = 0.22$ $r_{21} = 1.32$ $r_{32} = 1.3$ $\varphi_{ext21} = 1.3992$ $e_{a21} = 0.92\%$ $e_{ext21} = 17.5\%$

60 Degree, 8ft Diameter Bifurcations with 100% Split and Velocity of 30 ft/s

$\varphi_1 = 4.635225$ $\varphi_2 = 4.672336$ $\varphi_3 = 4.910739$

$GCI_{fine} = 0.15\%$ $p = 7.22$ $\varphi_{ext21} = 4.6295$

$r_{21} = 1.32$ $e_{a21} = 0.8\ \%$

$r_{32} = 1.3$ $e_{ext21} = 0.1\%$

GCI for Loss Coefficients(K) Through Run:

45 Degree, 4inch Diameter Bifurcations with 0% Split and Velocity of 45ft/s

Number of cells and associated φ:

$N1 = 3252707$ $N2 = 1429631$ $N3 = 627588$

$\varphi_1 = 0.2318517$ $\varphi_2 = 0.2343987$ $\varphi_3 = 0.2330053$

$GCI_{fine} = 1.66\%$ $p = 2.2$ $\varphi_{ext21} = 0.2288$

$r_{21} = 1.32$ $e_{a21} = 1.1\ \%$

$r_{32} = 1.32$ $e_{ext21} = 1.34\%$

45 Degree, 4inch Diameter Bifurcations with 40% Split and Velocity of 45ft/s

Number of cells and associated φ:

$\varphi_1 = 0.1073991$ $\varphi_2 = 0.1068417$ $\varphi_3 = 0.1019969$

$GCI_{fine} = 0.1\%$ $p = 7.88$ $\varphi_{ext21} = 0.1075$

$r_{21} = 1.32$ $e_{a21} = 0.52\%$

$r_{32} = 1.32$ $e_{ext21} = 0.1\%$

45 Degree, 4inch Diameter Bifurcations with 100% Split and Velocity of 45ft/s

$\varphi_1 = 0.3927751$ $\varphi_2 = 0.3905746$ $\varphi_3 = 0.3765108$

$GCI_{fine} = 0.1\%$ $p = 6.76$ $\varphi_{ext21} = 0.3932$

$r_{21} = 1.32$ $e_{a21} = 0.56\%$

$r_{32} = 1.32$ $e_{ext21} = 0.1\%$

45 Degree, 8ft Diameter Bifurcations with 0% Split and Velocity of 30ft/s

Number of cells and associated φ:

$N1 = 4667700$ $N2 = 2034836$ $N3 = 919487$

$\varphi_1 = 0.1582015$ $\varphi_2 = 0.1602987$ $\varphi_3 = 0.1589921$

$GCI_{fine} = 2.83\%$ $p = 1.67$ $\varphi_{ext21} = 0.1546$

$r_{21} = 1.32$ $e_{a21} = 1.33\%$

$r_{32} = 1.3$ $e_{ext21} = 2.32\%$

45 Degree, 8ftDiameter Bifurcations with 60% Split and Velocity of 30ft/s

Number of cells and associated φ:

$\varphi_1 = 0.1128146$ $\varphi_2 = 0.1116383$ $\varphi_3 = 0.1078844$

$GCI_{fine} = 0.5\%$ $p = 4.47$ $\varphi_{ext21} = 0.1133$

$r_{21} = 1.32$ $e_{a21} = 1.04\%$

$r_{32} = 1.3$ $e_{ext21} = 0.4\%$

45 Degree, 8ft Diameter Bifurcations with 100% Split and Velocity of 30ft/s

$\varphi_1 = 0.3520988$ $\varphi_2 = 0.3484998$ $\varphi_3 = 0.334194$

$GCI_{fine} = 0.4\%$ $p = 5.29$ $\varphi_{ext21} = 0.3532$

$r_{21} = 1.32$ $e_{a21} = 1.02\%$

$r_{32} = 1.3$ $e_{ext21} = 0.3\%$

35 Degree, 8ft Diameter Bifurcations with 0% Split and Velocity of 30ft/s

Number of cells and associated φ:

$N1 = 5089675$ $N2 = 2232012$ $N3 = 1004689$

$\varphi_1 = 0.1789999$ $\varphi_2 = 0.1817993$ $\varphi_3 = 0.1825619$

$GCI_{fine} = 0.79\%$ $p = 4.53$ $\varphi_{ext21} = 0.1779$

$r_{21} = 1.32$ $e_{a21} = 1.56\%$

$r_{32} = 1.3$ $e_{ext21} = 0.64\%$

35 Degree, 8ftDiameter Bifurcations with 60% Split and Velocity of 30ft/s

Number of cells and associated φ:

$\varphi_1 = 0.1133415$ $\varphi_2 = 0.1119801$ $\varphi_3 = 0.1080167$

$GCI_{fine} = 0.7\%$

$p = 4.08$

$r_{21} = 1.32$

$r_{32} = 1.3$

$\varphi_{ext21} = 0.114$

$e_{a21} = 1.2\ \%$

$e_{ext21} = 0.6\%$

35 Degree, 8ft Diameter Bifurcations with 100% Split and Velocity of 30ft/s

$\varphi_1 = 0.3365613$ $\varphi_2 = 0.3328245$ $\varphi_3 = 0.3187542$

$GCI_{fine} = 0.5\%$

$p = 5.04$

$r_{21} = 1.32$

$r_{32} = 1.3$

$\varphi_{ext21} = 0.3378$

$e_{a21} = 1.11\%$

$e_{ext21} = 0.4\%$

60 Degree, 8ft Diameter Bifurcations with 0% Split and Velocity of 30ft/s

Number of cells and associated φ:

$N1 = 4313371$ $N2 = 1865389$ $N3 = 853074$

$\varphi_1 = 0.1451039$ $\varphi_2 = 0.1465923$ $\varphi_3 = 0.1446092$

$GCI_{fine} = 3.69\%$

$p = 1.07$

$r_{21} = 1.32$

$r_{32} = 1.3$

$\varphi_{ext21} = 0.1408$

$e_{a21} = 1.03\%$

$e_{ext21} = 3.04\%$

60 Degree, 8ft Diameter Bifurcations with 60% Split and Velocity of 30ft/s

Number of cells and associated φ:

$\varphi_1 = 0.1110339$ $\varphi_2 = 0.1119801$ $\varphi_3 = 0.1050587$

$GCI_{fine} = 0.1\%$

$p = 7.57$

$r_{21} = 1.32$

$r_{32} = 1.3$

$\varphi_{ext21} = 0.1109$

$e_{a21} = 0.85\%$

$e_{ext21} = 0.1\%$

60 Degree, 8ft Diameter Bifurcations with 100% Split and Velocity of 30ft/s

$\varphi_1 = 0.3623041$ $\varphi_2 = 0.3603179$ $\varphi_3 = 0.3445916$

$GCI_{fine} = 0.1\%$

$p = 8.01$ $\varphi_{ext21} = 0.3625$

$r_{21} = 1.32$ $e_{a21} = 0.55\%$

$r_{32} = 1.3$ $e_{ext21} = 0.1\%$

GCI for Loss Coefficients(K) Through Branch:

45 Degree, 4inch Diameter Bifurcations with 0% Split and Velocity of 45ft/s

Number of cells and associated φ:

$N1 = 3252707$ $N2 = 1429631$ $N3 = 627588$

$\varphi_1 = 0.9906166$ $\varphi_2 = 0.9882723$ $\varphi_3 = 0.9779713$

$GCI_{fine} = 0.09\%$

$p = 5.39$ $\varphi_{ext21} = 0.9913$

$r_{21} = 1.32$ $e_{a21} = 0.24\%$

$r_{32} = 1.32$ $e_{ext21} = 0.07\%$

45 Degree, 4inch Diameter Bifurcations with 40% Split and Velocity of 45ft/s

Number of cells and associated φ:

$\varphi_1 = 0.6137707$ $\varphi_2 = 0.6091694$ $\varphi_3 = 0.5970653$

$GCI_{fine} = 0.6\%$

$p = 3.52$ $\varphi_{ext21} = 0.6166$

$r_{21} = 1.32$ $e_{a21} = 0.75\%$

$r_{32} = 1.32$ $e_{ext21} = 0.5\%$

45 Degree, 4inch Diameter Bifurcations with 100% Split and Velocity of 45ft/s

$\varphi_1 = 0.528047$ $\varphi_2 = 0.5241252$ $\varphi_3 = 0.516547$

$GCI_{fine} = 1\%$

$p = 2.4$ $\varphi_{ext21} = 0.5323$

$r_{21} = 1.32$ $e_{a21} = 0.74\%$

$r_{32} = 1.32$ $e_{ext21} = 0.8\%$

45 Degree, 8ft Diameter Bifurcations with 0% Split and Velocity of 30ft/s

Number of cells and associated φ:

$N1 = 4667700$ $N2 = 2034836$ $N3 = 919487$

$\varphi_1 = 0.962523$ $\varphi_2 = 0.9592166$ $\varphi_3 = 0.9472613$

$GCI_{fine} = 0.15\%$ $p = 4.93$ $\varphi_{ext21} = 0.9637$

$r_{21} = 1.32$ $e_{a21} = 0.34\%$

$r_{32} = 1.3$ $e_{ext21} = 0.12\%$

45 Degree, 8ftDiameter Bifurcations with 60% Split and Velocity of 30ft/s

Number of cells and associated φ:

$\varphi_1 = 0.4156313$ $\varphi_2 = 0.4095082$ $\varphi_3 = 0.3972102$

$GCI_{fine} = 1.6\%$ $p = 2.75$ $\varphi_{ext21} = 0.421$

$r_{21} = 1.32$ $e_{a21} = 1.47\%$

$r_{32} = 1.3$ $e_{ext21} = 1.3\%$

45 Degree, 8ft Diameter Bifurcations with 100% Split and Velocity of 30ft/s

$\varphi_1 = 0.430023$ $\varphi_2 = 0.4283104$ $\varphi_3 = 0.4168802$

$GCI_{fine} = 0.1\%$ $p = 7.22$ $\varphi_{ext21} = 0.4303$

$r_{21} = 1.32$ $e_{a21} = 0.4\%$

$r_{32} = 1.3$ $e_{ext21} = 0.1\%$

35 Degree, 8ft Diameter Bifurcations with 0% Split and Velocity of 30ft/s

Number of cells and associated φ:

$N1 = 5089675$ $N2 = 2232012$ $N3 = 1004689$

$\varphi_1 = 0.9331056$ $\varphi_2 = 0.9262502$ $\varphi_3 = 0.9118118$

$GCI_{fine} = 0.76\%$ $p = 2.88$ $\varphi_{ext21} = 0.9388$

$r_{21} = 1.32$ $e_{a21} = 0.73\%$

$r_{32} = 1.3$ $e_{ext21} = 0.61\%$

35 Degree, 8ftDiameter Bifurcations with 60% Split and Velocity of 30ft/s

Number of cells and associated φ:

$\varphi_1 = 0.344173$ $\varphi_2 = 0.3370126$ $\varphi_3 = 0.3251476$

$GCI_{fine} = 3.6\%$ $p = 1.99$ $\varphi_{ext21} = 0.354$

$r_{21} = 1.32$ $e_{a21} = 2.08\%$

$r_{32} = 1.3$ $e_{ext21} = 2.8\%$

35 Degree, 8ft Diameter Bifurcations with 100% Split and Velocity of 30ft/s

$\varphi_1 = 0.3987564$ $\varphi_2 = 0.395082$ $\varphi_3 = 0.3927877$

$GCI_{fine} = 2.1\%$ $p = 1.57$ $\varphi_{ext21} = 0.4056$

$r_{21} = 1.32$ $e_{a21} = 0.92\%$

$r_{32} = 1.3$ $e_{ext21} = 1.7\%$

60 Degree, 8ft Diameter Bifurcations with 0% Split and Velocity of 30ft/s

Number of cells and associated φ:

$N1 = 4313371$ $N2 = 1865389$ $N3 = 853074$

$\varphi_1 = 0.9782009$ $\varphi_2 = 0.9748493$ $\varphi_3 = 0.9628302$

$GCI_{fine} = 0.14\%$ $p = 5.02$ $\varphi_{ext21} = 0.9793$

$r_{21} = 1.32$ $e_{a21} = 0.34\%$

$r_{32} = 1.3$ $e_{ext21} = 0.11\%$

60 Degree, 8ftDiameter Bifurcations with 60% Split and Velocity of 30ft/s

Number of cells and associated φ:

$\varphi_1 = 0.5514542$ $\varphi_2 = 0.5448755$ $\varphi_3 = 0.5289326$

$GCI_{fine} = 0.9\%$ $p = 3.55$ $\varphi_{ext21} = 0.5553$

$r_{21} = 1.32$ $e_{a21} = 1.19\%$

$r_{32} = 1.3$ $e_{ext21} = 0.7\%$

60 Degree, 8ft Diameter Bifurcations with 100% Split and Velocity of 30ft/s

$\varphi_1 = 0.5665106$ $\varphi_2 = 0.5594096$ $\varphi_3 = 0.5480746$

$GCI_{fine} = 2.1\%$

$p = 1.99$

$r_{21} = 1.32$

$r_{32} = 1.3$

$\varphi_{ext21} = 0.576$

$e_{a21} = 1.25\%$

$e_{ext21} = 1.7\%$

Appendix D

Experimental Uncertainty

What follows is the SMath Studio print out of the calculation tabulated in Table 3.3 and 3.4.

Experimental Uncertainty

Equation for K:

$$K = \frac{2 \cdot g \cdot \left(\frac{P_1 - P_2}{\gamma} + \frac{V_1^2 - V_2^2}{2 \cdot g} \right)}{V_1^2}$$

Derivation of the uncertainty of K equation:

Derivatives:

$$\frac{d}{dP_1} K = \frac{2 \cdot g}{\gamma \cdot V_1^2} \qquad \frac{d}{dP_2} K = -\frac{2 \cdot g}{\gamma \cdot V_1^2}$$

$$dKdP1 = \frac{2 \cdot g}{\gamma \cdot V_1^2} \qquad dKdP2 = -\frac{2 \cdot g}{\gamma \cdot V_1^2}$$

$$\frac{d}{dV_1} K = -\frac{2 \cdot \left(2 \cdot \left(P_1 - P_2 \right) \cdot g + \gamma \cdot \left(\left(V_1 - V_2 \right) \cdot \left(V_1 + V_2 \right) - V_1^2 \right) \right)}{V_1^3 \cdot \gamma}$$

$$dKdV1 = -\frac{2 \cdot \left(2 \cdot \left(P_1 - P_2 \right) \cdot g + \gamma \cdot \left(\left(V_1 - V_2 \right) \cdot \left(V_1 + V_2 \right) - V_1^2 \right) \right)}{V_1^3 \cdot \gamma}$$

$$\frac{d}{dV_2} K = -\frac{2 \cdot V_2}{V_1^2} \qquad dKdV2 = -\frac{2 \cdot V_2}{V_1^2}$$

$$\frac{d}{d\gamma} K = -\frac{2 \cdot \left(P_1 - P_2 \right) \cdot g}{\gamma^2 \cdot V_1^2} \qquad dKd\gamma = -\frac{2 \cdot \left(P_1 - P_2 \right) \cdot g}{\gamma^2 \cdot V_1^2}$$

Putting it all together to get the Uncertainty of K:

$$U_K = \sqrt{U_{P1}^2 \cdot dKdP1^2 + U_{P2}^2 \cdot dKdP2^2 + U_{V1}^2 \cdot dKdV1^2 + U_{V2}^2 \cdot dKdV2^2 + U_\gamma^2 \cdot dKd\gamma^2}$$

Uncertainty of each of the components to calculating K.
First time through for 0% split flow for K through the run

Uncertainty of the Area:

$D = 4.026\,in$ $U_D = \frac{D}{4000}$ $U_D = 0.0001\,ft$ $A = \pi \cdot \frac{D^2}{4}$

$U_A = A \cdot \sqrt{4 \cdot \left(\frac{U_D}{D}\right)^2}$ $U_A = 0.0000442\,ft^2$

Uncertainty of the Velocity:

Gy

$M_1 = 1861.125 \frac{gal}{min}$ $M_2 = 1861.125 \frac{gal}{min}$

$U_{M1} = 0.0025 \cdot M_1$ $U_{M2} = 0.0025 \cdot M_2$

$U_{M1} = 4.65281 \frac{gal}{min}$ $U_{M2} = 4.65281 \frac{gal}{min}$

$V_1 = \frac{M_1}{A}$ $V_1 = 46.9048 \cdot \frac{1}{s}\,ft$ $V_2 = \frac{M_2}{A}$ $V_2 = 46.9048 \cdot \frac{1}{s}\,ft$

$U_{V1} = V_1 \cdot \sqrt{\left(\frac{U_{M1}}{M_1}\right)^2 + \left(\frac{U_A}{A}\right)^2}$ $U_{V2} = V_2 \cdot \sqrt{\left(\frac{U_{M2}}{M_2}\right)^2 + \left(\frac{U_A}{A}\right)^2}$

$U_{V1} = 0.1196 \cdot \frac{1}{s}\,ft$ $U_{V2} = 0.1196 \cdot \frac{1}{s}\,ft$

Uncertainty of the Pressure:

$P_1 = 8.3813\,psi$ $U_{P1} = 0.001 \cdot P_1$ $U_{P1} = 0.0084\,psi$

$P_2 = 5.7000\,psi$ $U_{P2} = 0.001 \cdot P_2$ $U_{P2} = 0.0057\,psi$

Uncertainty of the γ:

$\gamma = 62.31572 \frac{lbf}{ft^3}$ $U_\gamma = \frac{\gamma}{62000}$ $U_\gamma = 0.001 \frac{lbf}{ft^3}$ $g = 32.174 \frac{ft}{s^2}$

Uncertainty of K:

$$dKdP1 = \frac{2 \cdot g}{\gamma \cdot V_1^{\,2}} \qquad dKdP2 = -\frac{2 \cdot g}{\gamma \cdot V_1^{\,2}}$$

$$dKdP1 = 0.0005 \frac{ft^{\,2}}{lbf} \qquad dKdP2 = -0.0005 \frac{ft^{\,2}}{lbf}$$

$$dKdV1 = -\frac{2 \cdot \left(2 \cdot \left(P_1 - P_2\right) \cdot g + \gamma \cdot \left(\left(V_1 - V_2\right) \cdot \left(V_1 + V_2\right) - V_1^{\,2}\right)\right)}{V_1^{\,3} \cdot \gamma}$$

$$dKdV1 = 0.0349\, s\, ft^{-1}$$

$$dKdV2 = -\frac{2 \cdot V_2}{V_1^{\,2}} \qquad dKdV2 = -0.0426\, s\, ft^{-1}$$

$$dKd\gamma = -\frac{2 \cdot \left(P_1 - P_2\right) \cdot g}{\gamma^{\,2} \cdot V_1^{\,2}} \qquad dKd\gamma = -0.0029 \frac{ft^{\,3}}{lbf}$$

$$U_K = \sqrt{U_{P1}^{\,2} \cdot dKdP1^{\,2} + U_{P2}^{\,2} \cdot dKdP2^{\,2} + U_{V1}^{\,2} \cdot dKdV1^{\,2} + U_{V2}^{\,2} \cdot dKdV2^{\,2} + U_{\gamma}^{\,2} \cdot dKd\gamma^{\,2}}$$

$$U_{K\_percent} = \frac{U_K}{K} \cdot 100$$

0% Flow K through Run:

$K = 0.1812$ $U_K = 0.00663$ $\boxed{U_{K\_percent} = 3.66\%}$

10% Flow K through Run:

$M_1 = 1993.50 \frac{gal}{min}$ $M_2 = 1804.25 \frac{gal}{min}$

$P_1 = 2.1938\, psi$ $P_2 = 3.7125\, psi$

$K = 0.0914$ $U_K = 0.00624$ $\boxed{U_{K\_percent} = 6.83\%}$

20% Flow K through Run:

$M_1 = 1973.0 \frac{gal}{min}$ $M_2 = 1578.4 \frac{gal}{min}$

$P_1 = 3.09375 psi$ $P_2 = 7.9125 psi$

$K = 0.0702$ $U_K = 0.00578$ $\boxed{U_{K\_percent} = 8.23\%}$

30% Flow K through Run:

$M_1 = 1913.75 \frac{gal}{min}$ $M_2 = 1344.75 \frac{gal}{min}$

$P_1 = 5.75625 psi$ $P_2 = 12.46875 psi$

$K = 0.0772$ $U_K = 0.00541$ $\boxed{U_{K\_percent} = 7.01\%}$

40% Flow K through Run:

$M_1 = 1894.75 \frac{gal}{min}$ $M_2 = 1146.25 \frac{gal}{min}$

$P_1 = 6.76875 psi$ $P_2 = 14.98125 psi$

$K = 0.0985$ $U_K = 0.00508$ $\boxed{U_{K\_percent} = 5.15\%}$

50% Flow K through Run:

$M_1 = 1795 \frac{gal}{min}$ $M_2 = 906.5 \frac{gal}{min}$

$P_1 = 10.8 psi$ $P_2 = 19.66875 psi$

$K = 0.1006$ $U_K = 0.00504$ $\boxed{U_{K\_percent} = 5.01\%}$

60% Flow K through Run:

$M_1 = 1696.25 \frac{gal}{min}$ $M_2 = 670.5 \frac{gal}{min}$

$P_1 = 15.65625 psi$ $P_2 = 23.79375 psi$

$K = 0.1816$ $U_K = 0.00484$ $\boxed{U_{K\_percent} = 2.66\%}$

70% Flow K through Run:

$M_1 = 1638.75 \frac{gal}{min}$ $M_2 = 494.5 \frac{gal}{min}$

$P_1 = 18.1875 psi$ $P_2 = 26.08125 psi$

$K = 0.2208$ $U_K = 0.00487$ $\boxed{U_{K\_percent} = 2.2\%}$

80% Flow K through Run:

$M_1 = 1588.5 \frac{gal}{min}$ $M_2 = 319.775 \frac{gal}{min}$

$P_1 = 20.475 psi$ $P_2 = 27.75 psi$

$K = 0.2845$ $U_K = 0.00486$ $\boxed{U_{K\_percent} = 1.71\%}$

90% Flow K through Run:

$M_1 = 1527.5 \frac{gal}{min}$ $M_2 = 153.725 \frac{gal}{min}$

$P_1 = 23.19375 psi$ $P_2 = 29.5125 psi$

$K = 0.3559$ $U_K = 0.005$ $\boxed{U_{K\_percent} = 1.4\%}$

100% Flow K through Run:

$M_1 = 1434 \frac{gal}{min}$ $M_2 = 0 \frac{gal}{min}$

$P_1 = 27.20625 psi$ $P_2 = 32.309375 psi$

$K = 0.419$ $U_K = 0.00565$ $\boxed{U_{K\_percent} = 1.35\%}$

0% Flow K through Branch:

$M_1 = 1861.125 \frac{gal}{min}$ $M_2 = 0 \frac{gal}{min}$

$P_1 = 8.38125 psi$ $P_2 = 8.45625 psi$

$K = 0.9949$ $U_K = 0.00081$ $\boxed{U_{K\_percent} = 0.08\%}$

10% Flow K through Branch:

$M_1 = 1993.5 \frac{gal}{min}$ $M_2 = 189.25 \frac{gal}{min}$

$P_1 = 2.19375 psi$ $P_2 = 3.525 psi$

$K = 0.9126$ $U_K = 0.00051$ $\boxed{U_{K\_percent} = 0.06\%}$

20% Flow K through Branch:

$M_1 = 1973 \frac{gal}{min}$ $M_2 = 394.6 \frac{gal}{min}$

$P_1 = 3.09375 psi$ $P_2 = 6 psi$

$K = 0.7852$ $U_K = 0.00119$ $\boxed{U_{K\_percent} = 0.15\%}$

30% Flow K through Branch:

$M_1 = 1913.75 \frac{gal}{min}$ $M_2 = 569 \frac{gal}{min}$

$P_1 = 5.75625 psi$ $P_2 = 9.3 psi$

$K = 0.6851$ $U_K = 0.00181$ $\boxed{U_{K\_percent} = 0.26\%}$

40% Flow K through Branch:

$M_1 = 1894.75 \frac{gal}{min}$ $M_2 = 748.5 \frac{gal}{min}$

$P_1 = 6.76875 psi$ $P_2 = 10.93125 psi$

$K = 0.5725$ $U_K = 0.00247$ $\boxed{U_{K\_percent} = 0.43\%}$

50% Flow K through Branch:

$M_1 = 1795 \frac{gal}{min}$ $M_2 = 888.5 \frac{gal}{min}$

$P_1 = 10.8 psi$ $P_2 = 14.83125 psi$

$K = 0.4621$ $U_K = 0.0033$ $\boxed{U_{K\_percent} = 0.71\%}$

60% Flow K through Branch:

$M_1 = 1696.25 \frac{gal}{min}$ $M_2 = 1025.75 \frac{gal}{min}$

$P_1 = 15.65625 psi$ $P_2 = 18.1125 psi$

$K = 0.4345$ $U_K = 0.00395$ $\boxed{U_{K\_percent} = 0.91\%}$

70% Flow K through Branch:

$M_1 = 1638.75 \frac{gal}{min}$ $M_2 = 1144.25 \frac{gal}{min}$

$P_1 = 18.1875 psi$ $P_2 = 19.33125 psi$

$K = 0.4127$ $U_K = 0.00453$ $\boxed{U_{K\_percent} = 1.1\%}$

80% Flow K through Branch:

$M_1 = 1588.5 \frac{gal}{min}$ $M_2 = 1268.725 \frac{gal}{min}$

$P_1 = 20.475 psi$ $P_2 = 19.9125 psi$

$K = 0.4143$ $U_K = 0.00515$ $\boxed{U_{K\_percent} = 1.24\%}$

90% Flow K through Branch:

$M_1 = 1527.5 \frac{gal}{min}$ $M_2 = 1373.775 \frac{gal}{min}$

$P_1 = 23.19375 psi$ $P_2 = 20.6625 psi$

$K = 0.4451$ $U_K = 0.00589$ $\boxed{U_{K\_percent} = 1.32\%}$

100% Flow K through Branch:

$M_1 = 1434 \frac{gal}{min}$ $M_2 = 1434 \frac{gal}{min}$

$P_1 = 27.20625 psi$ $P_2 = 22.70625 psi$

$K = 0.5123$ $U_K = 0.00696$ $\boxed{U_{K\_percent} = 1.36\%}$